Ecological Monographs, 76(4), 2006, pp. 481–502

MACROALGAL SPORE DISPERSAL IN COASTAL ENVIRONMENTS: MECHANISTIC INSIGHTS REVEALED BY THEORY AND EXPERIMENT

Brian Gaylord,[1,5] Daniel C. Reed,[2] Peter T. Raimondi,[3] and Libe Washburn[4]

[1]*Bodega Marine Laboratory and Section of Evolution and Ecology, University of California at Davis, P.O. Box 247, Bodega Bay, California 94923 USA*
[2]*Marine Science Institute, University of California at Santa Barbara, Santa Barbara, California 93106 USA*
[3]*Department of Biology, University of California at Santa Cruz, Santa Cruz, California 95064 USA*
[4]*Department of Geography and Institute for Computational Earth Systems Science, University of California at Santa Barbara, Santa Barbara, California 93106 USA*

Abstract. Passively dispersing propagules are often transported across a range of scales, with impacts on local processes tied to the density of settlement, and on regional processes influencing population connectivity. This dual set of effects has spurred research targeting both short- and long-distance ends of the dispersal spectrum. To date, however, dispersal distributions have been rigorously quantified primarily in terrestrial plants with seeds. Dispersal distributions in the ocean are by comparison poorly defined. This limitation arises with particular force in the habitat-forming giant kelp, *Macrocystis pyrifera*, where complex coastal flows affect self-fertilization and inbreeding depression near to a source, as well as propagule delivery dictating recovery of locally extinct populations farther away.

Here we use a combination of theoretical and experimental approaches to examine spore dispersal in *Macrocystis*. Results from a physically based model, parameterized via field-measured hydrodynamics, are compared to settlement data gathered at the same experimental site using spore collectors positioned around solitary kelps and an experimental kelp forest. Theoretical and empirical findings are synthesized, and the ability of simple phenomenological expressions to represent short- and long-distance spore dispersal is examined.

Results demonstrate that short-distance dispersal patterns quantified over brief durations are noisy due to stochastic effects of turbulence. Waves can further smear distributions, reducing distinctions between dispersal from point sources (e.g., solitary kelps) vs. area sources (e.g., entire forests). Temporally averaged dispersal distributions follow a lognormal–Gaussian form that is explicitly coupled to current speed. Analyses based on this phenomenological expression provide first-order benchmarks useful in several contexts. Calculations suggest a tremendous rate of spore release in *Macrocystis*, exceeding 10^8 spores per individual per day. Routine fertilization and recruitment appear possible at distances beyond 1 km from many beds, modulated by current speed, forest size, and the duration of viability of gamete-producing life stages derived from spores. Within *Macrocystis* forests where settlement densities are high, selfing levels on the order of 10% or more may arise. These characteristics influence patterns of propagule supply, population connectivity, and inbreeding in this key nearshore seaweed, while also revealing trends in the mechanics of propagule dispersal more generally.

Key words: connectivity; dispersal ecology; fluid transport; giant kelp; larval dispersal; Macrocyctis pyrifera; *marine propagule transport; metapopulations; Santa Barbara Channel, California, USA; self-fertilization; spore dispersal; theoretical and empirical approaches to dispersal.*

Introduction

Wind or water-mediated dispersal of propagules (seeds, spores, larvae) can play a critical role in determining the distribution, dynamics, connectivity, and genetic structure of populations of sessile organisms. In terrestrial systems, attention has often focused on species' dispersal "kernels," the probability density function that describes the likelihood that a propagule will disperse to a particular location (e.g., Clark et al. 1999, 2001, Nathan and Muller-Landau 2000, Levin et al. 2003). An emerging set of phenomenological kernel representations match observed patterns of propagule transport (mostly as related to seed dispersal by wind), yet are simple enough to embed in general theoretical models. These mathematical forms are used in studies with both short- and long-distance focus to address a variety of issues, including rates of species advance and invasion, metapopulation dynamics, spatially explicit species interactions, and local adaptation and population genetics.

In contrast to the growing body of work on terrestrial dispersal kernels, far less is known about dispersal

Manuscript received 7 September 2005; revised 15 March 2006; accepted 1 June 2006. Corresponding Editor: P. D. Steinberg.
[5] E-mail: bpgaylord@ucdavis.edu

patterns in the sea. Indeed, most theoretical studies, the majority of which focus on planktonic animal larvae, have invoked a "common pool" model. This model assumes that propagules are mixed homogenously and redistributed uniformly along the shore. A subset of studies have made more detailed assumptions about dispersal kernels (Possingham and Roughgarden 1990, Richards et al. 1995, Cowen et al. 2000, Gaylord and Gaines 2000, Lockwood et al. 2002, Siegel et al. 2003), but the difficulty of tracking microscopic propagules has slowed field validation. Naturally, the above information gap is widely recognized and has spurred the development of new tools. For example, trace elements have been used to back-estimate natal sites of recruits (e.g., Swearer et al. 1999, DiBacco and Levin 2000, Zacherl et al. 2003), and genetic methods have been employed to define scales of dispersal from characteristics of population heterogeneity (e.g., Palumbi 1995, Grosberg and Cunningham 2001, Wares et al. 2001, Kinlan and Gaines 2003, Sotka et al. 2004).

There is another level of understanding that is also vital but has remained even more elusive. Unlike with dispersal of seeds on land where there is a tradition of incorporating physical elements in kernel parameterizations (e.g., seed release heights and fall velocities, air currents, statistics of wind gusts, Okubo and Levin 1989, Greene and Johnson 1989, 1996, Andersen 1991, Nathan et al. 2001, 2002, Tackenberg 2003, Soons et al. 2004), phenomenological representations of marine dispersal have not been as effectively linked to nearshore ocean processes. A number of important physical factors have been identified, including upwelling/relaxation phenomena (Roughgarden et al. 1988, Wing et al. 1995, 1998, Garland et al. 2002) and internal waves and bores (Pineda 1991, Shanks 1995, Leichter et al. 1996), but it has not been generally possible to develop mechanistic descriptors of propagule transport that can be reduced to simple mathematical forms suitable for guiding ecological theory.

Such limitations are problematic in a general sense, but they become acutely disadvantageous when attempting to understand dispersal in important marine species such as the giant kelp, *Macrocystis pyrifera*. This large alga forms productive forests along many of the world's temperate coasts (Wormersley 1954, North 1971), provides habitat and refuge for hundreds of associated species, and, like other kelps (see, e.g., Duggins et al. 1989), is consumed by many of them. The population dynamics of *Macrocystis* is also connected intimately to the dispersal of its propagules. Forests of this species are often spatially disjunct, separated by sand flats. They are also vulnerable to physical and biological disturbance due to large waves (Dayton et al. 1984, 1992, Seymour et al. 1989), poor growing conditions (Dayton and Tegner 1984, Edwards 2004), and intense grazing (Ebeling et al. 1985, Harrold and Reed 1985). The regional persistence of a kelp metapopulation composed of multiple forests (Reed et al. 2006) may therefore be maintained via source–sink dynamics involving local extinctions and recoveries driven by propagule delivery from neighboring kelp beds. Such source–sink relationships may be further altered by high rates of local settlement, which increases inbreeding with resultant reductions in per capita fecundity (Raimondi et al. 2004). Together these effects indicate the necessity for a physically based understanding of propagule dispersal throughout the entire kernel. Although previous studies have indicated that many *Macrocystis* propagules (i.e., spores) settle within a few meters of the adult kelp plant, and that a substantial fraction are also transported hundreds to thousands of meters (Anderson and North 1966, Gaylord et al. 2002, Reed et al. 2004, 2006), there remain many unaddressed details regarding the shapes of dispersal distributions and their relationship to hydrodynamic processes.

Here, focusing explicitly on *Macrocystis* but also with an eye to the general issue of marine propagule transport, we employ a combination of theoretical and empirical approaches to examine dispersal in shallow coastal habitats. Our goal is threefold: (1) to develop a mechanistic understanding of how nearshore hydrodynamics impact the movement of propagules like algal spores, (2) to evaluate the potential for simple phenomenological distributions to appropriately represent these processes, and (3) to illustrate the utility of such phenomenological distributions for guiding other work. Findings point to both the complexity of dispersal in nearshore areas, as well as to underlying relationships among dispersal distance and key physical phenomena that bear on the population ecology of *Macrocystis* and other coastal species.

Physical Processes Influencing Nearshore Dispersal

Although ocean currents are analogous to air currents in many ways, there are at least three important factors that distinguish fluid-mediated dispersal in marine environments from terrestrial dispersal by wind. First, propagules in the sea have mass densities much closer to that of the surrounding fluid, leading to a tendency for them to fall more slowly. Second, there is no strict upper bound on how high propagules can be carried above the ground by wind; in the ocean, by contrast, the water's surface provides a defined constraint. Third, ocean gravity waves propagate on the water's surface whereas there is no exact analogue to these waves in land-based systems.

Such elements of marine vs. terrestrial transport can be quantified and distinguished as follows. As either air or water flows over a solid surface, fluid near the surface is slowed to produce a boundary layer, within which velocities often follow a logarithmic form (Clauser 1956; also see Denny 1988, Greene and Johnson 1989, Eckman 1990, Nathan et al. 2001, Soons et al. 2004),

$$u_c = \frac{u_{*c}}{\kappa} \ln\left(\frac{z}{z_0}\right) \quad (1)$$

where u_c is the horizontal speed of the current at height z above the substratum, κ is von Karman's constant (equal to 0.4), and u_{*c} is the current shear velocity, a measure of the magnitude of friction-like shear stresses operating at the fluid–substratum interface that are generated by the current. The parameter z_0 is a length scale related to the height of roughness elements of the substratum. Although typically applied to steady currents in isolation, Eq. 1 can also hold in marine systems where ocean waves are present, with a key adjustment: z_0 becomes larger because wave–current interactions elevate the total shear stress at the substratum, making the substratum appear in a functional sense rougher than it actually is (Grant and Madsen 1986).

In addition to their effects on horizontal currents, and their production of bidirectional flows, waves also influence rates of vertical mixing. This effect is perhaps equally important in the context of dispersal since vertical movement is what dictates how long propagules remain suspended and therefore how far they can be swept by horizontal flows while they remain aloft. Traditionally, the rate of turbulent vertical mixing is modeled in terms of an eddy diffusivity, K_t, which is often assumed to increase linearly away from the substratum (e.g., Okubo and Levin 1989, Anderson 1991):

$$K_t = \kappa u_{*c} z. \tag{2}$$

The presence of waves in marine systems, however, enhances mixing within a relatively thin wave boundary layer that is embedded within the much thicker current boundary layer. As a result, the overall turbulent-mixing profile becomes dependent on multiple processes operating with different scales of motion, the effects of which can be represented as follows (Wiberg and Smith 1983):

$$K_t = \kappa z \left[u_{*c}^2 \exp\left(-\frac{2z}{l_c}\right) + u_{*w}^2 \exp\left(-\frac{2z}{l_w}\right) \right]^{1/2} \tag{3}$$

where u_{*w} is the maximum shear velocity associated with just the waves, and l_c and l_w are length scales of mixing associated with the current and waves, respectively. In practice, there is also a molecular-diffusion component that only becomes important extremely close to the seabed (McNair et al. 1997), producing an overall eddy diffusivity of

$$K = \frac{\nu}{2} + \sqrt{\left(\frac{\nu}{2}\right)^2 + (K_t)^2} \tag{4}$$

where ν is the kinematic viscosity of the fluid, which accounts for the molecular effects. Note that if ν is neglected and if waves are absent ($u_{*w} = 0$), Eq. 4 approaches the form of Eq. 2, at least for small values of z. Under these conditions, the current profile, which becomes slightly nonlogarithmic when Eq. 4 is used, analogously converges to Eq. 1.

A Theoretical Framework for Spore Dispersal

Physically based model

A treatment of boundary-layer mixing in the context of spore dispersal has been presented earlier by Gaylord et al. (2002). However, in that largely conceptual study, wave and current conditions were assumed fixed. Although some aspects of current variability were addressed by Reed et al. (2006), important idealizations remained. In this study, we implement a model that incorporates the full suite of physical factors dominating dispersal: variable current speeds and directions, changes in flow with depth, and shifting wave heights, wave periods, and directions of wave propagation.

The model operates in four parts. The first part sets the initial location of spores in space as they are "released" by kelp plants in the model. These spores begin at a model height of 42 cm above the seafloor, consistent with field measurements (Gaylord et al. 2002). The initial horizontal locations are set by the positions of real plants studied during accompanying field experiments (see *Field experiments*, below). Two configurations are used: a "solitary kelp-plant array," where three replicate adults are spaced 50 m apart in a line, and a "kelp-bed array" where 64 individuals are positioned in an 8×8 grid with 3-m spacing, covering a 21×21 m square region of seafloor (Fig. 1). For the solitary kelp-plant array, 300 model spores are released every hour, distributed over the three adults in proportion to values of plant-specific fecundity measured for the field individuals. In the case of the kelp-bed array, 1000 model spores are released every hour, likewise distributed over the 64 individuals in proportion to measured plant-specific fecundities. Note that the exact number of spores released in the model is immaterial since the approach is designed to provide insight only into relative (not absolute) levels of settlement across space. The assumed steady rate of spore release reflects patterns presented in Graham (2003), which suggest little diel periodicity.

The second part of the model quantifies nonlinear interactions between waves and currents, which affect vertical mixing and horizontal velocities in lower regions of the current boundary layer. The eddy diffusivity, K, defined in terms of the current- and wave-associated shear velocities by Eqs. 3 and 4, is also linked to current- and wave-generated velocity gradients by the relations

$$u_{*c}^2 = K\left(\frac{\partial u_c}{\partial z}\right) \qquad u_{*w}^2 = K\left(\frac{\partial u_w}{\partial z}\right)_{max} \tag{5}$$

where $\partial u_c/\partial z$ is the vertical velocity gradient of the current at the seafloor, and $(\partial u_w/\partial z)_{max}$ is the maximum wave-associated vertical velocity gradient at the seafloor. Eq. 5 and the eddy diffusivity of Eqs. 3 and 4 are then matched to ensure that they are all consistent (Appendix A). Ultimately, this linkage dictates how currents and waves interact to alter mixing rates and flow speeds across depth.

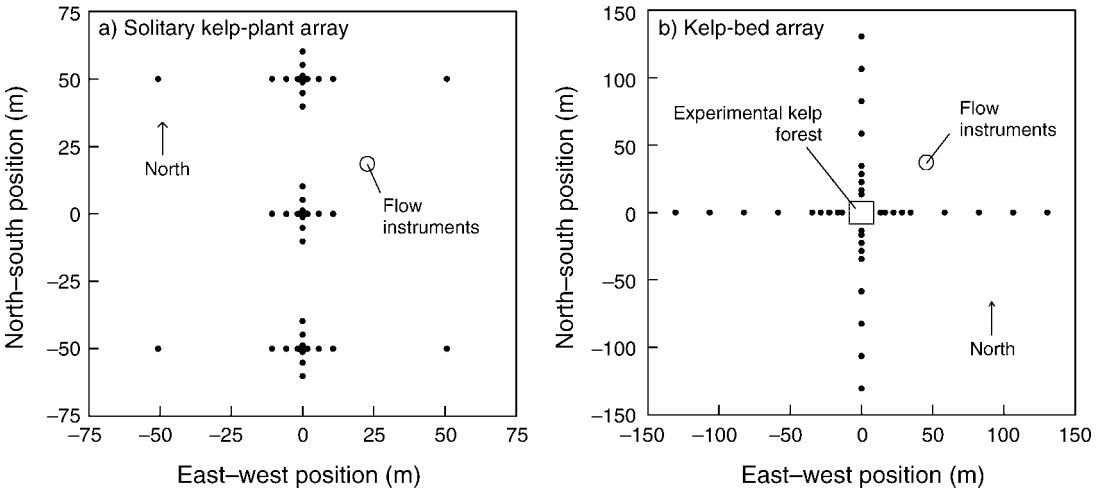

FIG. 1. Configuration of the slide sampling arrays employed for the (a) solitary kelp-plant experiment and (b) kelp-bed experiment. Each point represents the location of a glass microscope slide used as a spore collector. The approximate position of an acoustic Doppler current profiler (ADCP; used to measure currents across the water column) and an acoustic Doppler velocimeter (ADV; used to measure waves) is also indicated. Note that the shoreline in this region runs east–west.

In the third part of the model, the profile of vertical mixing is combined with a random-walk approach (McNair et al. 1997) to simulate vertical movement of spores. The method tracks each spore as it takes numerous turbulence-mediated steps until it contacts the seafloor at $z = 0$. The probability of moving up or down (p or q, respectively) by a distance δ during a short time interval T_{step} is given by

$$p = \frac{2K + \left(\frac{dK}{dz} - s\right)\delta}{4K} \qquad q = \frac{2K - \left(\frac{dK}{dz} - s\right)\delta}{4K} \qquad (6)$$

where s is the spore sinking speed in still water as quantified by Gaylord et al. (2002), and $\delta = (2KT_{\text{step}})^{1/2}$. A random-number generator determines the directional "decision" at each step. In addition, spores are swept horizontally by currents present at their elevation in the water column, as well as vertically and horizontally by the wave motions at that elevation. Note that a redundant representation of molecular effects in the related analysis of Gaylord et al. (2002) is eliminated in Eq. 6, although it had an imperceptible effect on results.

The final part of the model involves hourly updating of hydrodynamic conditions throughout the dispersal period of interest. All model components are determined from measured data (there are no "free" variables) interpolated onto a 1-h temporal grid. Currents in mid-water are defined using field-measured flows, while velocities near the seafloor outside the measurement region are derived from the near-logarithmic profile (akin to Eq. 1; see Appendix A) associated with the eddy diffusivity of Eq. 4. Velocities above the measurement region near the water's surface are set equal to flow values from the highest measurement location. Orbital wave velocities at given positions in the water column are determined from linear wave theory (Denny 1988), assuming for simplicity a monochromatic wave train with amplitude and period set by the measured significant wave height and dominant wave period. Note that this approach accounts for the second-order shoreward drift produced by waves (Monismith and Fong 2004).

Phenomenological forms for dispersal

In addition to examining spore dispersal from multiple-plant arrays, we also model dispersal from a true point source represented by a single kelp plant. This plant releases 100 spores per hour, across the full range of hydrodynamic conditions measured during the study. Predicted settlement outcomes from this simplest-of-possible source configurations provide a useful data set for evaluating the ability of idealized phenomenological expressions to represent dispersal.

Traditionally, phenomenological dispersal forms have been based on power law expressions or equations from the exponential family of curves (including the negative exponential, Gaussian, and Weibull; Levin et al. 2003, Greene et al. 2004). More recently, however, two additional forms have gained broader support, namely, Clark's 2Dt distribution (Clark et al. 1999) and the lognormal distribution (Stoyan and Wagner 2001, Greene et al. 2004):

$$p(r) = 2a(b-1)r(1+ar^2)^{-b} \qquad \text{(2Dt)} \qquad (7)$$

$$p(r) = \frac{1}{a\sqrt{2\pi}r}\exp\left[-\frac{(\ln r - \ln b)^2}{2a^2}\right] \qquad \text{(lognormal)} \qquad (8)$$

where a and b are fitted parameters and the integral of either expression from $r = 0$ to positive infinity equals 1 (i.e., both are proper probability density functions). Note that Eqs. 7 and 8 are one-dimensional "distance distributions" (Nathan and Muller-Landau 2000) in that

they quantify the probability of a propagule settling within an infinitesimally thin annulus at distance r, rather than the probability of a spore settling in an infinitesimal two-dimensional area at position (x, y).

Parameters a and b are determined by fitting the probability density functions of Eqs. 7 and 8 to the predicted point-source dispersal patterns using maximum-likelihood approaches. The resulting mathematical expressions are integrated to produce cumulative probability distributions (i.e., the probabilities that spores disperse less than particular distances), which are compared to model-predicted cumulative distributions estimated as

$$P(r) = \frac{R}{N+1} \tag{9}$$

where the predicted dispersal distances have been sorted in ascending order such that R corresponds to the rank of a particular radial distance (r) and N is the total number of distances (see also Gaylord et al. 1994). Both the phenomenological and model-predicted cumulative probability values are then transformed into Gaussian "Z values" (i.e., standard normal deviates; Sokal and Rohlf 1995), which causes distributions with a Gaussian character to plot as straight lines.

Field Experiments

Study organism

Dispersal in *Macrocystis* is linked to aspects of its biology. The conspicuous and commonly observed stage of giant kelp is the sporophyte, which produces tiny male and female spores near its base on specialized blades called sporophylls (Neushul 1963). Following release, the spores disperse and settle, eventually developing into free-living microscopic male and female gametophytes. The gametophytes in turn produce eggs and sperm that fertilize to form a sporophyte. The connection between this life history and flow-driven dispersal is twofold. First, because the ability of sperm to find eggs is spatially limited, fertilization only occurs if the male and female spores from which the gametophytes are derived settle at relatively high densities (>1 spore/mm^2; Reed 1990). This effect decouples patterns of dispersal (spore transport to a given location) from recruitment (appearance of juvenile sporophytes at a given location), since sufficient increases in the magnitude of a spore source can increase settlement densities throughout the distribution, enabling fertilization and thus recruitment farther into the dispersal tail (Reed et al. 1997, 2004, 2006). Second, because gametophytes arising from the same parent sporophyte produce compatible gametes, patterns of dispersal adjacent to source individuals may influence levels of inbreeding (Raimondi et al. 2004).

Field site

Field experiments examining *Macrocystis* spore dispersal were conducted within the Santa Barbara Channel off the coast of Carpinteria, California, USA (34°23′33″ N, 119°32′38″ W). The shoreline in this area is oriented along an east–west axis and the study site was located ~1 km from the beach in water of 10-m depth, in the middle of an extensive sand flat. The closest kelp beds were >1 km upcoast and downcoast, which minimized interference from other spore sources. Currents at the site derive from tides, winds, and regional pressure gradients, with mean currents averaged over weeks exhibiting speeds of 0.02 m/s (Reed et al. 2006) and peak velocities reaching ~0.5 m/s (Harms and Winant 1998, Washburn et al. 1999). Winter waves from the North Pacific are usually smaller than those present on fully exposed, outer coasts.

Hydrodynamic measurements

Flow conditions specific to the field experiments at Carpinteria were detailed using an acoustic Doppler current profiler (ADCP) and an acoustic Doppler velocimeter (ADV), deployed in five major blocks between April 1998 and August 1999. These instruments recorded at a rate and resolution sufficient for empirically defining the hydrodynamic context for dispersal at the site, and parameterizing the accompanying theoretical model. The ADCP measured current speed and direction from a height of 1.5 m above the seafloor to 7 m above it in 0.5-m-depth bins, burst sampling at 0.5 Hz for 80 points every 15 min. The ADV sampled velocity and pressure at 2 Hz for 2048 points, every 8 h, to quantify wave conditions. Significant wave heights and dominant wave periods were calculated from the pressure records using standard Fourier methods (e.g., Gaylord 1999, Gaylord et al. 2003). Wave direction was determined from the orientation of the largest principal axis of the wave velocities (Emery and Thomson 2001).

Solitary kelp-plant experiment

The fieldwork examining spore dispersal in *Macrocystis* proceeded in two experiments, paralleling the modeling efforts. The first experiment focused on dispersal away from individual plants, configured identically to the solitary kelp-plant array in the model. The field setup was accomplished by transplanting three reproductively mature *Macrocystis* adults to the Carpinteria sand flat, near the hydrodynamic instruments (Fig. 1). These kelps were secured to concrete emplacements ($120 \times 20 \times 20$ cm) positioned 50 m apart along a north–south transect oriented perpendicular to shore, a spacing that enabled each of the three plants to function to first order as an isolated, replicate spore source.

Around each plant, vertical plastic posts (2 cm in diameter) were driven into the sand, positioned in an X-shaped array. The apex of each post protruded 15 cm above the seafloor. A small platform bolted to the apex of the post supported a frosted glass microscope slide, which acted as settlement substrate for the kelp spores released by each adult (see also Reed et al. 1988). The

slides were located at distances of 1.2, 1.7, 5.7, and 10.7 m to the east and west of the center of each plant, and at distances of 0.7, 1.2, 5.2, and 10.2 m to the north and south of the center of each plant (Fig. 1a). Additional slides were also located 50.7 m to the east and west of both the farthest inshore plant and the farthest offshore plant.

The three plants were monitored on a periodic basis and their level of fecundity was determined by counting the number of sporophylls with fertile sori, and multiplying this number by the average sorus area on each sporophyll (Reed et al. 1996). Individuals were replaced with a new fecund adult as they became senescent or nonreproductive. The glass microscope slides and their attached spores were also swapped out on a 2–3 day cycle. On each sampling date the microscope slides and attached spores were retrieved by divers, placed in filtered seawater, and kept in the dark during the 1-h transit time to the laboratory. The spores were then placed in culture at 15°C and examined under a microscope within one week to score the density of spore settlement. Densities were estimated by counting the average number of female gametophytes (which form from female spores only, but which are densely pigmented and therefore more easily identified) in 20 replicate microscope fields of view, each covering 1.66 mm^2 of the slide's surface. This deployment–retrieval cycle was continued from April 1998 to May 1999, with the data examined here encompassing the subset of 55 deployments (of 76 total) that were accompanied by hydrodynamic measurements.

Kelp-bed experiment

The second field experiment, spanning 15 deployments from June through July of 1999, focused on dispersal around 64 individuals making up an experimental forest corresponding to the kelp-bed array of the model (Fig. 1b). This experimental forest provided a means of examining transport away from a spore source distributed over a finite area, to complement data from the replicate point sources of the solitary kelp-plant array. Each plant in the kelp-bed array was attached to a concrete emplacement as described for the solitary kelp-plant experiment. Due to the greater size of the potential spore source associated with the kelp-bed array, however, the sampling configuration was modified to include microscope slides at distances of 3, 6, 12, 18, 24, 48, 72, 96, and 120 m from each edge of the experimental kelp bed. Fecundities of plants were again monitored, slides were retrieved on a 2–3 day cycle, and spore densities were determined in the laboratory.

Results

General hydrodynamic characteristics

Depth-averaged currents at the field site oscillated tidally at daily and twice-daily frequencies, with magnitudes between 0 and 0.35 m/s (Fig. 2). Standard deviations of the depth-averaged velocity, computed over each 2–3 day deployment, ranged from 0.02 to 0.10 m/s during the solitary kelp-plant experiment and 0.03 to 0.06 m/s during the kelp-bed experiment. Certain portions of the water column also deviated substantially from the depth-averaged values, and such velocity shear was incorporated into the theoretical model. Several strong flow events occurred, particularly during the solitary kelp-plant experiment, when rapid southeastward currents prevailed (visible in Fig. 2 as a combination of positive values in the east–west panel and negative values in the north-south panel). Significant wave heights spanned 0.25 m to almost 1.5 m during the solitary kelp-plant experiment, with greater variability and most larger wave events occurring during the winter and spring. Wave conditions were milder during the kelp-bed experiment, with significant wave heights ranging from 0.25 to 0.7 m.

Model-predicted spore dispersal patterns

Solitary kelp-plant array.—Overall dispersal distributions predicted for the solitary kelp-plant array exhibited spore transport in a variety of directions, as well as radially symmetric dispersal (Fig. 3a, upper row). In all cases, maximum predicted dispersal distances extended as far as several kilometers. Closer to the source, directionality in spore settlement was often reduced compared to that of the entire distribution (Fig. 3a, lower row). Even in cases when directional asymmetries in short-distance dispersal did arise, they did not always track the direction of asymmetry of the corresponding long-distance distributions. Much of the spatial pattern visible in short-distance regions also derived from differences in settlement densities around certain individuals in the three-plant array. This feature was a consequence of the variation in measured fecundity among plants, rather than the result of physical factors. It is also of note that although the three model plants were employed as rough replicates, there was modest exchange between adjacent distributions, although it occurred in lower density portions of the kernels.

Kelp-bed array.—As for the solitary kelp-plant array, predicted dispersal patterns varied across kelp-bed deployments, with directional transport occurring in some cases but not others. Spore densities around the kelp-bed array (Fig. 3b, lower row) reached higher levels at equivalent distances from the source than for the solitary plants, partially due to the greater concentration of source individuals and partially due to the higher aggregate rate of spore release (1000 model spores/h vs. 300 spores/h). Maximum predicted dispersal distances, however, again extended several kilometers (Fig. 3b, upper row). This consistency arose because maximum dispersal distances are limited by how far water itself can move during a deployment. Even if a spore remains suspended for the whole 2–3 days and only settles at the last moment, it cannot disperse farther than the maximal net excursion of the flow.

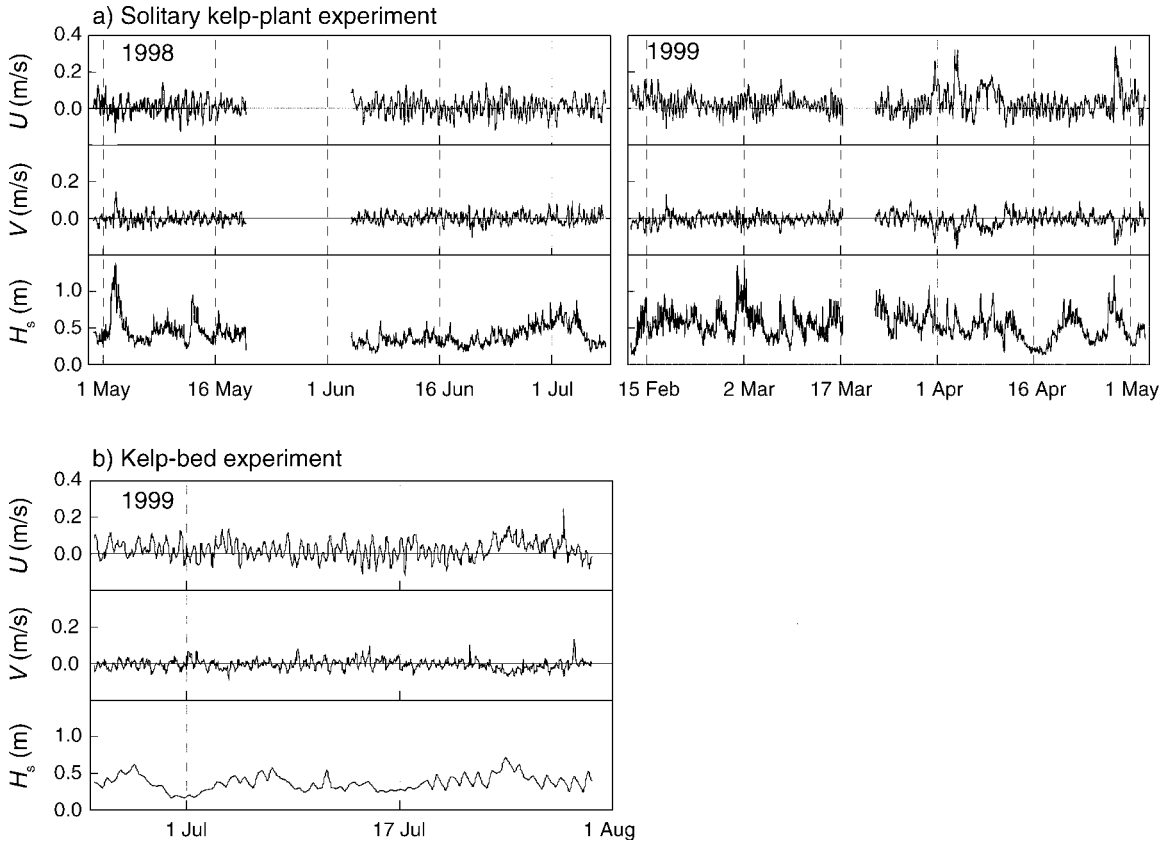

FIG. 2. Summary of hydrodynamic data recorded during the (a) solitary kelp-plant experiment and (b) kelp-bed experiment. Depth-averaged currents in the east–west (U) and north–south (V) directions are shown through time, as is the significant wave height (H_s).

Variability among deployment-specific patterns

Solitary kelp-plant array.—"Transects" can also be run through the short-distance predicted distributions for direct comparison to field-measured patterns. In the case of the solitary kelp-plant array (Fig. 4a), each predicted transect sampled a series of 0.25 m wide (circumferentially) by 0.1 m long (radially) regions surrounding the equivalent model locations to where microscope slides were positioned in the field. The size of the regions was determined in such a way that the numbers of sampled model spores resembled the numbers from the field experiments. Resulting model-predicted spore patterns averaged over the three replicate plants declined rapidly with distance, at comparable rates along east–west and north–south axes (Fig. 4a, upper row). The average measured spore patterns showed an analogous pattern, with densities typically falling to <1 spore per microscope field of view at a distance of 50.7 m (Fig. 4a, lower row). Despite the general similarities in shape of the predicted and measured transects, however, the dispersal curves exhibited considerable spikiness so that there was not a close deployment-by-deployment correspondence between the relative magnitudes or locations of their peaks.

Kelp-bed array.—Transects through the predicted distributions for the kelp-bed array (Fig. 4b) counted model spores settling in 1.25 m wide (circumferentially) by 0.5 m long (radially) areas corresponding to where slides were positioned in the field. Again, the size of these areas was selected to produce settlement curves with approximately the same number of spores as were found in the field experiment. As in the solitary kelp-plant experiment, predicted densities around the kelp-bed array dropped rapidly from the spore source (Fig. 4b, upper row), and dispersal along east–west and north–south transects was often, but not always, similar. Measured spore patterns exhibited analogous trends (Fig. 4b, lower row), although there was again substantial spikiness and little correspondence between the predicted and measured distributions on a deployment-by-deployment basis.

Effects of spore source geometry

The example results of Fig. 4 encompass only a subset of all of the solitary kelp-plant and kelp-bed deployments, respectively (see Appendices B and C for data from remaining deployments). The model transects also counted only spores predicted to settle in the vicinity of

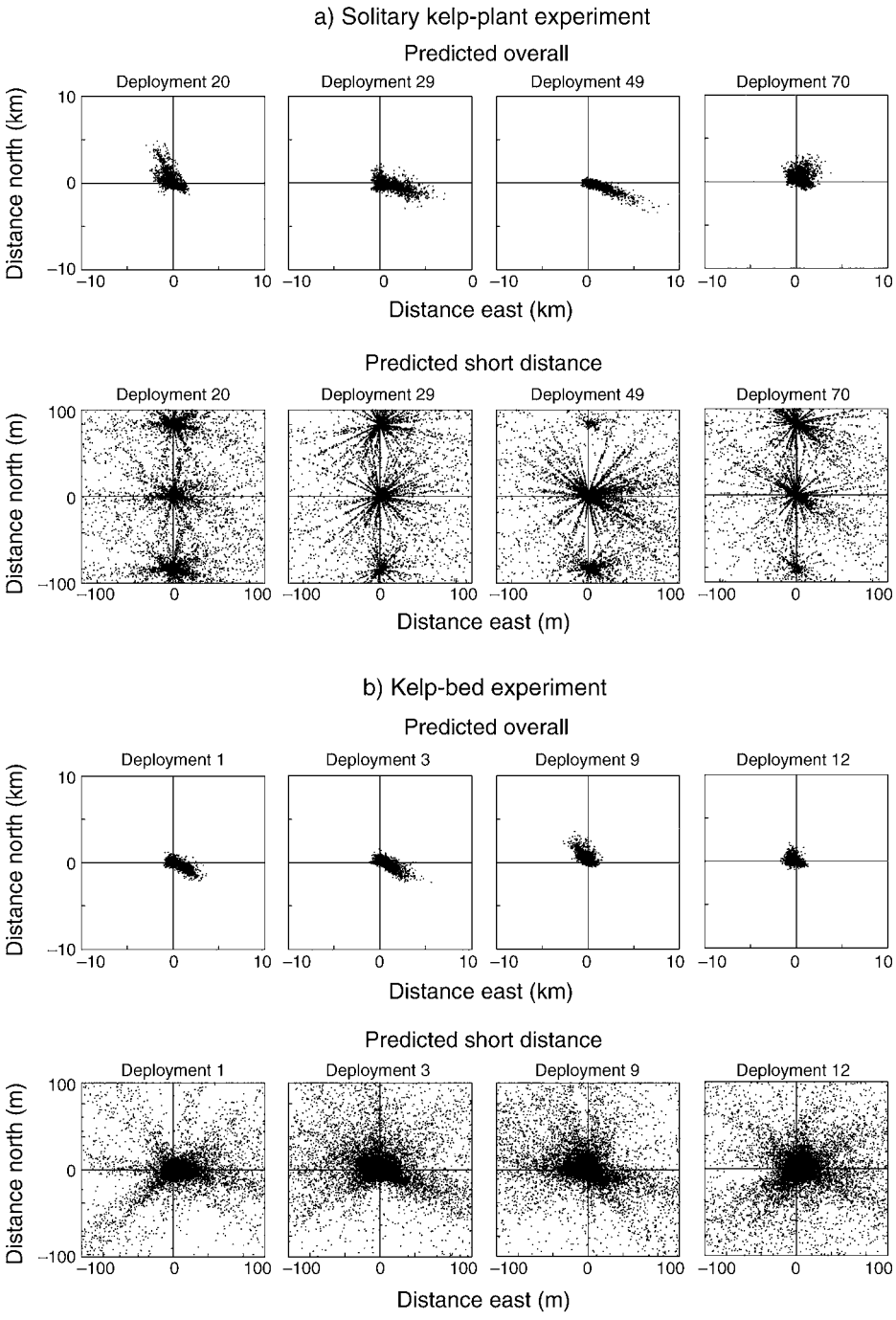

FIG. 3. Examples of predicted dispersal patterns from four model deployments of the (a) solitary kelp-plant experiment and (b) kelp-bed experiment. The panels in the upper row of each experiment depict the overall long-distance patterns, via an overhead view. Panels in the lower row of each experiment show short-distance patterns that result from "zooming in" on the overall patterns. The dimensions of the axes on the short-distance plots correspond to the spatial extent of the accompanying field measurements.

the slide positions used in the field sampling. Such predictions can be expanded by filling in areas between the slide positions to better understand aggregate patterns.

For the solitary kelp-plant array, coherent trends emerge when all spores predicted to settle along the 0.25-m-wide swaths that extend east and west, or north and south, from the central individual of the three-plant

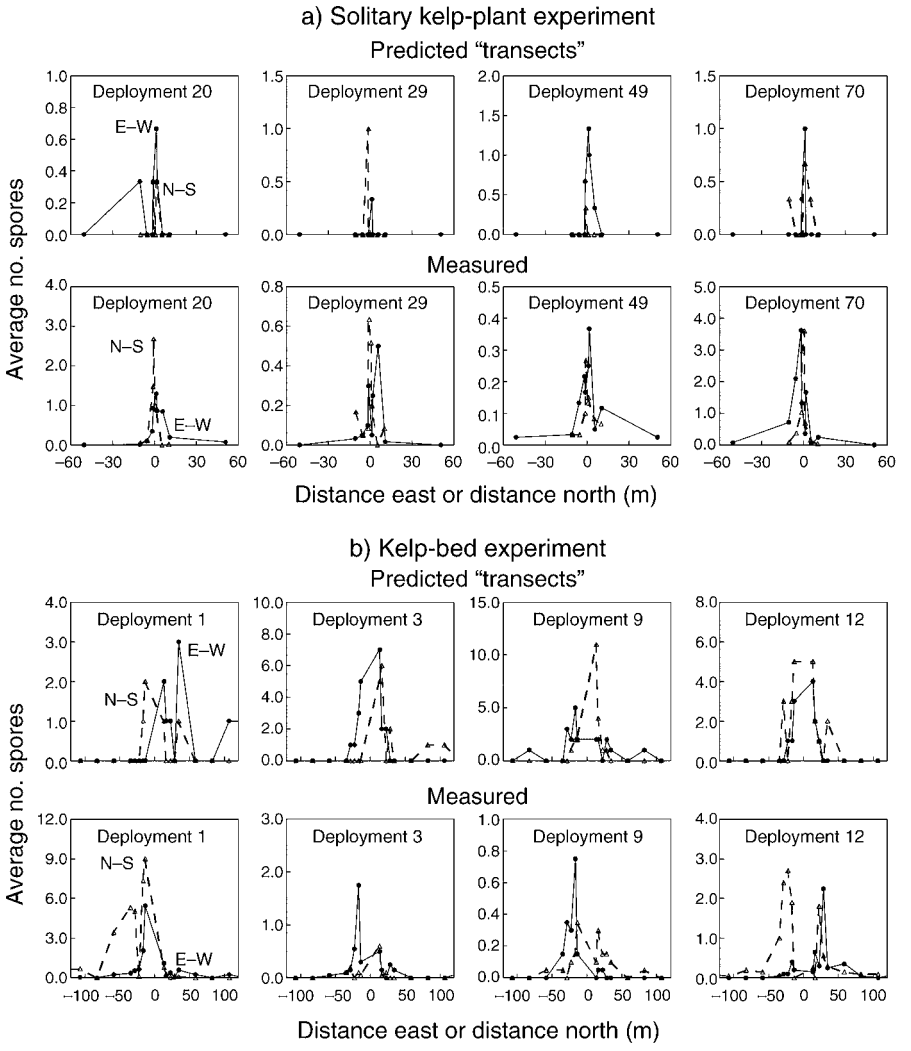

FIG. 4. Examples of predicted and measured "transects" through spore dispersal distributions from four deployments during the (a) solitary kelp-plant experiment and (b) kelp-bed experiment. Solid lines are the east–west distributions, and dashed lines are the north–south distributions. Note that during the solitary kelp-plant experiment, just the east–west transects had slides at 50.7 m, so the north–south data extend only to ~10 m. Values on the *y*-axes of the measured curves indicate the mean number of female spores averaged over 20 microscope fields of view (each 1.66 mm^2).

array are tallied (Fig. 5a). For instance, the band of dispersal histograms from the 55 deployments is nearly centered on zero and is essentially symmetric around its midpoint. The east–west portion of the predicted dispersal kernel is also weakly convex near the source, with decreased settlement occurring immediately adjacent to the plant (Fig. 5a, upper panel).

Somewhat different patterns arise for the 15 kelp-bed deployments when model-predicted histograms are assembled from spore counts along the 1.25-m-wide continuous swaths that extend east and west, or north and south, from the center of the model forest (Fig. 5b). In this case, there is no indication of a central dip in the dispersal distribution near the source. This finding is perhaps expected for the kelp-bed array since distributed area sources in terrestrial systems also exhibit dispersal curves with single broad peaks (Greene and Johnson 1996, Nathan et al. 2001).

Comparison of aggregate measured and predicted patterns

The measured and model-predicted spore dispersal patterns of Figs. 3–5 can also be averaged over all deployments to resolve underlying trends in their relationship. This procedure reveals that the average measured and model-predicted patterns are quite similar, both for the solitary kelp-plant experiment and the kelp-bed experiment (Fig. 6). For instance, regressions of measured vs. predicted distribution values from each directional axis exhibit R^2 values of 0.76 (east–west; $P < 0.001$) and 0.95 (north–south; $P < 0.001$) for the solitary kelp-plant array (Fig. 6a), and R^2 values of 0.67

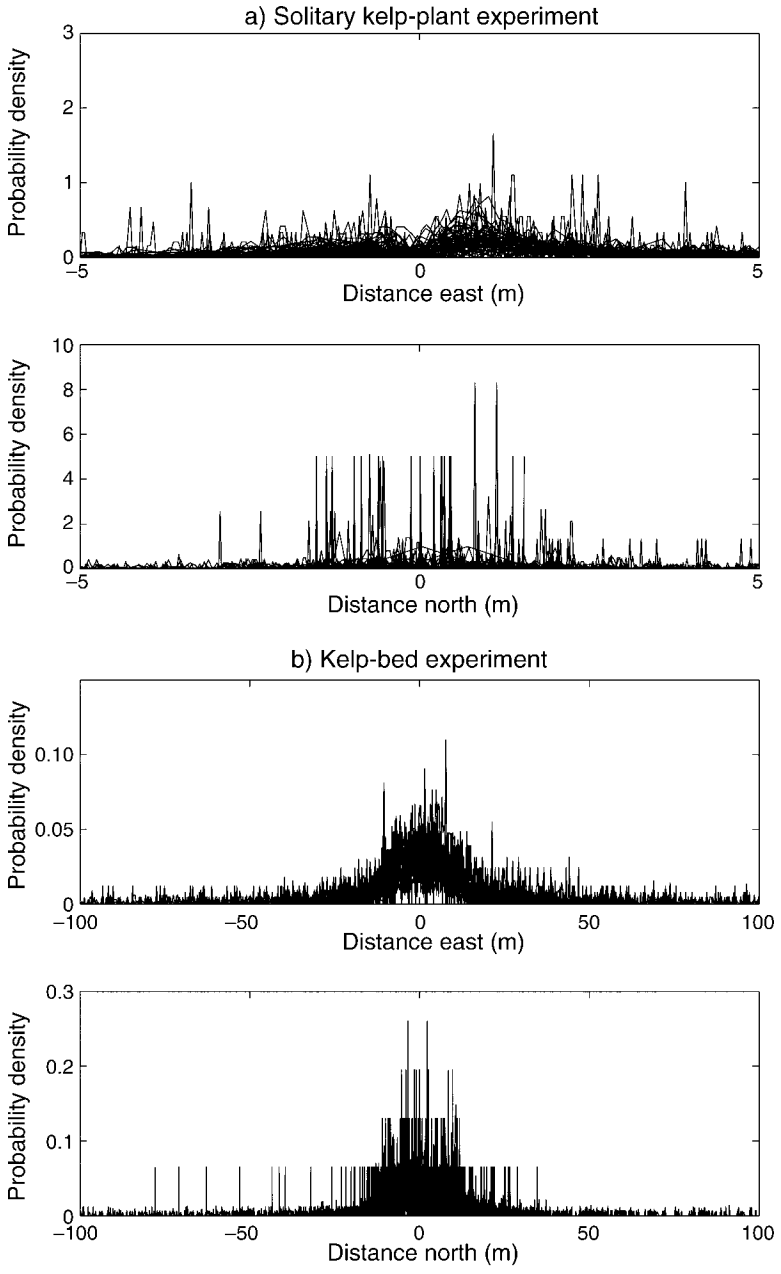

FIG. 5. Model-predicted probability density functions for settlement across all deployments. (a) Solitary kelp-plant experiment, depicting results for the full set of 55 deployments. All spores predicted to settle within a continuous, 0.25-m-wide swath extending east and west, or north and south from the origin are tallied. (b) Kelp-bed experiment, depicting results for the full set of 15 deployments. All spores predicted to settle within a continuous, 1.25-m-wide swath extending east and west, or north and south from the origin are tallied. Distributions are estimated using 5000-bin histograms.

(east–west; $P < 0.001$) and 0.49 (north–south; $P < 0.001$) for the kelp-bed array (Fig. 6b).

The correspondence between model and field results apparent in Fig. 6 is echoed by a related analysis that considers indices related to deployment-specific patterns. One such index is the centroid, essentially the average position of spore settlement within the sampling array, computed as follows:

$$\bar{x} = \frac{\sum(nx)}{\sum n} \qquad \bar{y} = \frac{\sum(ny)}{\sum n} \tag{10}$$

where n is the number of spores settling at a particular position (x, y), and $\sum n$ is the total number of spores collected during a given deployment. In these expressions, the x-axis is assumed to run east–west and the y-axis is assumed to run north–south. Thus, a negative x-

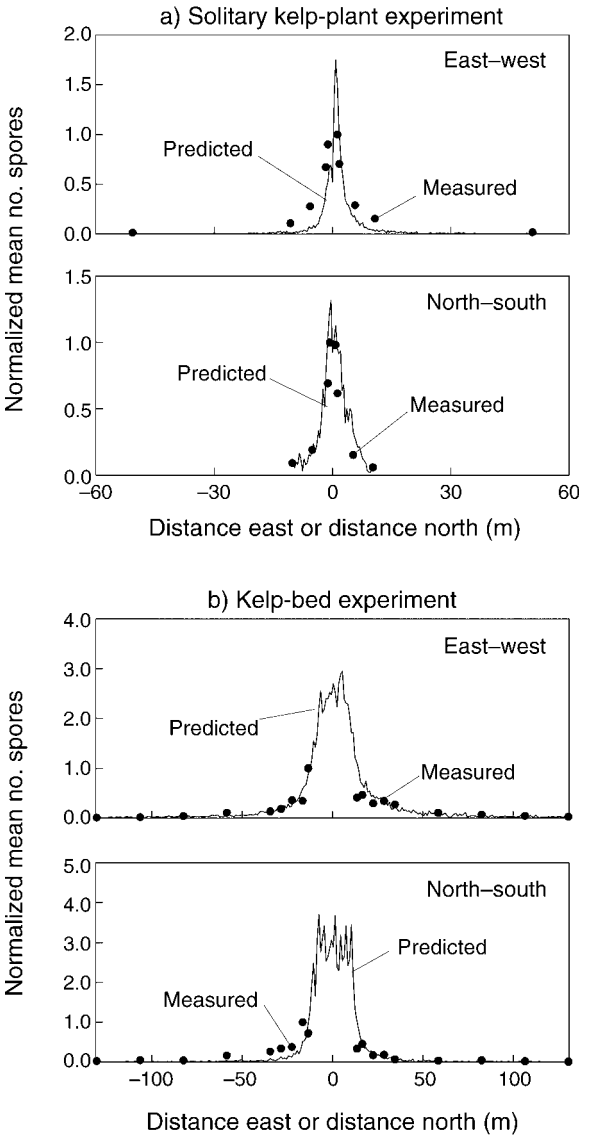

FIG. 6. Comparison of the average model-predicted and measured dispersal distributions, along both east–west and north–south axes, for the (a) solitary kelp-plant experiment and (b) kelp-bed experiment. The measured distributions are normalized by their peak values, while the predicted distributions are normalized such that the mean of their values at positive and negative distances corresponding to this slide position equals 1.0. This procedure scales the measured and predicted distributions so that they have similar magnitudes at locations where settlement was highest and estimates of the curves are most robust. Although the exact normalization values are essentially arbitrary, it is only relative levels across a distribution's extent that are of interest. Note that the lack of measured data points near the central peaks of the distributions in (b) does not imply a reduced degree of match, but simply reflects the fact that spore collectors were located exclusively outside the boundaries of the experimental forest.

centroid (x) means that spore settlement is weighted to the west of the origin, while a positive y-centroid ($\bar{y}$) indicates that spore settlement is weighted to the north, and vice versa. Undertaking these calculations using spore results of the same kind as those presented in Fig. 4 reveals that predicted and measured centroid distributions are not significantly different, for either the solitary kelp-plant or the kelp-bed experiment (Kolmogorov-Smirnov, $P > 0.05$ for either east–west and north–south directions; Fig. 7). This finding again indicates a close correspondence between model output and field data.

Given that spore dispersal in *Macrocystis* is driven by fluid transport, one might expect deployment-by-deployment centroids to be linked in a simple way to representative hydrodynamic factors. However, there is sufficient variability in short-distance settlement pat-

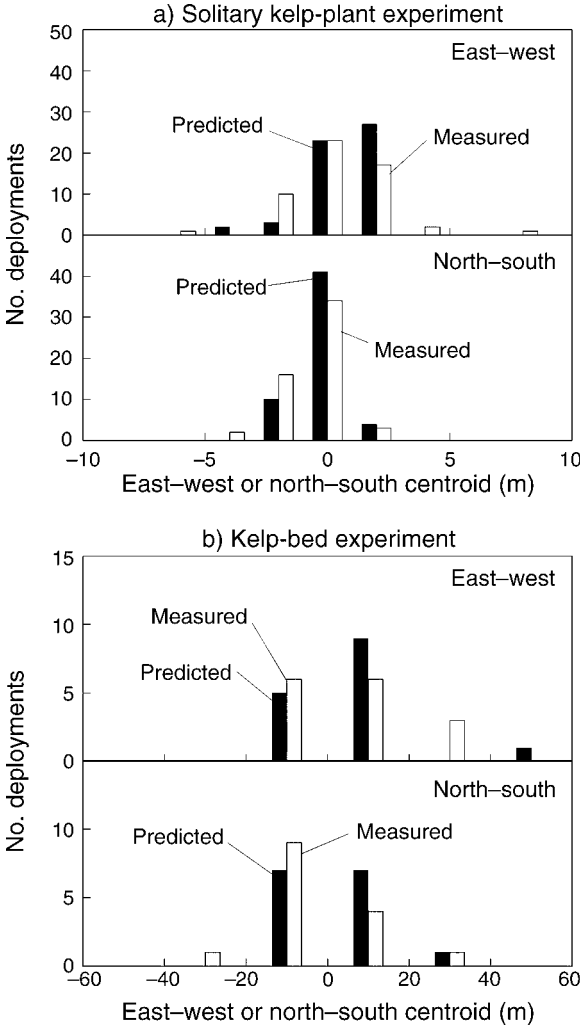

FIG. 7. Comparison of measured and predicted centroid histograms, computed over the dimensions of the slide sampling arrays, for the (a) solitary kelp-plant experiment and (b) kelp-bed experiment.

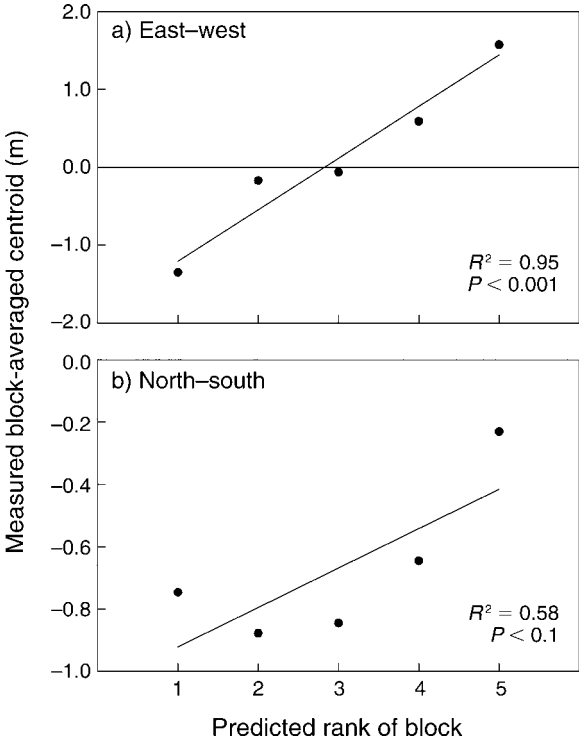

FIG 8. Patterns that emerge when measured centroids are compared to predictions of the physically based model. (a) Measured east–west centroid values increase with rank in accordance with model expectations. (b) A similar trend for the north–south centroid values exhibits a reduced degree of significance, likely due to effects of waves. Data are from the solitary kelp-plant experiment.

terns that deployment-specific measured centroids are uncorrelated with any obvious deployment-specific hydrodynamic quantity, including mean flow speed, mean current direction, standard deviation in velocity, wave height, wave direction, standard deviation in wave height, and wave period ($P > 0.05$ for all univariate and multivariate analyses performed). The notion that short-distance dispersal distributions cannot be explicitly linked to hydrodynamic conditions is dispelled, however, by the finding that even slight directional trends in the measured centroids are predicted by the physically based model, likely because it accounts for layered, nonlinear interactions. If measured centroids from the solitary kelp-plant experiment are sorted and averaged across five separate five-deployment blocks distributed over the 55 deployments, the east–west measured block-averaged centroids increase with the rank of the predicted block-averaged centroids (rank 1 = lowest, 5 = highest) in accordance with model expectations (Fig. 8a). This finding reaffirms the relevance of oceanographic processes in short-distance dispersal, even in view of the variability that characterizes the short-distance dispersal patterns on a deployment-by-deployment basis.

Effects of waves over short distances and currents over long distances

The reduced significance of the regression for the north–south centroids in Fig. 8b likely can also be ascribed to flow. Bidirectional velocities produced by waves are often faster than accompanying currents, and can sweep spores several meters in a few seconds. This feature smears short-distance dispersal distributions along the axis of wave propagation, which at the Carpinteria (California, USA) field site, aligns with a north–south axis. This smearing adds additional variation that can obscure pattern. For example, although there was only a hint of a central dip in the solitary kelp-plant distributions (Fig. 5a), such dips emerge clearly when effects of orbital wave transport are removed from the model (Fig. 9a). Orbital wave effects, in contrast, play little role in influencing dispersal patterns of the kelp-bed array (note similarity of Fig. 9b to Fig. 5b), since the distributed nature of the spore source already prevents convexity in the short-distance portion of the kernel.

In contrast to the subtlety of links between flow and dispersal in short-distance transport, trends in long-distance dispersal are closely tied to current speed. Indeed, the dimensions of the predicted overall dispersal footprint, which we index in terms of the maximum radial dispersal distance, is strongly connected to the mean depth-averaged current (Fig. 10). This finding is consistent with the notion that the farthest-dispersing spores are those that remain suspended for essentially the entire deployment, thereby tracking the net velocity and thus the net displacement of flow. The maximum predicted dispersal distance is also correlated with the sum of the depth-averaged standard deviations of cross-shore and alongshore velocities (Fig. 10). This pattern indicates that extended dispersal occurs both when mean flows are faster, and when currents vary substantially. In practice, these two physical factors are rarely fully independent since a slight directional bias of a large-amplitude oscillation, as occurs during spring tides, can produce a greater mean than a fractionally equivalent bias of a lower amplitude oscillation, as occurs during neap tides. This property may have important implications for dispersal of algae, invertebrates, and fishes that release their propagules on a lunar cycle.

Utility of phenomenological forms

In addition to revealing connections between hydrodynamics and dispersal, the physically based model also yields insight into the ability of phenomenological expressions to represent spore dispersal. The relevant parameter values for a and b in Eqs. 7 and 8 are given in Table 1. Fig. 11 compares the model-predicted cumulative dispersal distributions from the point source to the average phenomenological expressions that derive from fitting Eqs. 7 and 8 to the aggregate model data. Three average phenomenological curves are shown; the 2Dt,

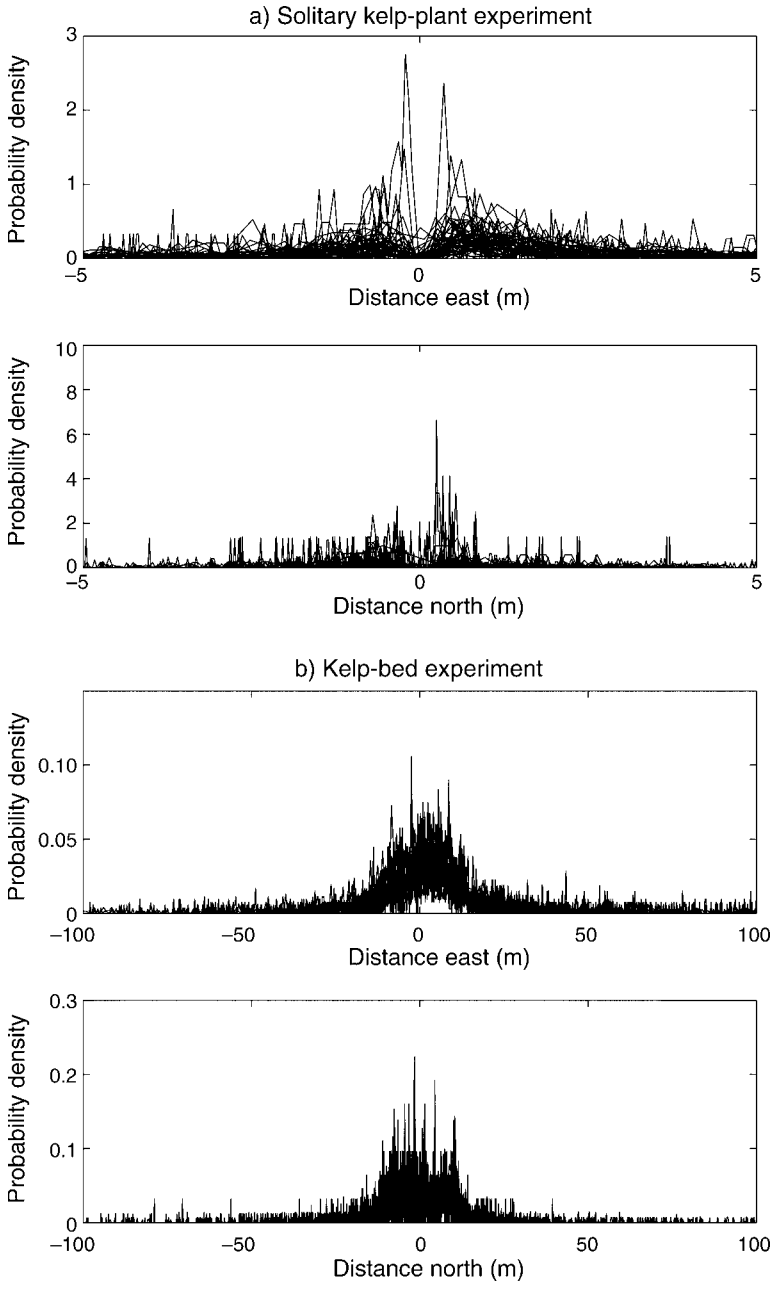

FIG. 9. Predicted dispersal patterns as in Fig. 5, except without the effects of orbital transport due to waves. Note the emergence of a clearer dip at the origin for the solitary kelp-plant experiment.

the lognormal, and a composite form that will be addressed below (see *Discussion*). Results reveal that although the model-predicted and average phenomenological curves overlap near the spore source, the average phenomenological expressions do not fit the wide range of tails predicted for different deployments.

In this regard, short-distance and long-distance regions of the model-predicted distributions behave differently. The tails have distinct slopes but are nearly linear when plotted on a probability scale, consistent with a Gaussian behavior (Fig. 11a). In contrast, short-distance regions all fall on a similar line but are curvilinear (Fig. 11a). It is only after the standard normal deviates (Z values) of the short-distance regions are re-plotted against the logarithm of distance that they exhibit near-linear behavior (Fig. 11b). This trend indicates that dispersal close to the plant operates as a lognormal process, consistent with Eq. 8.

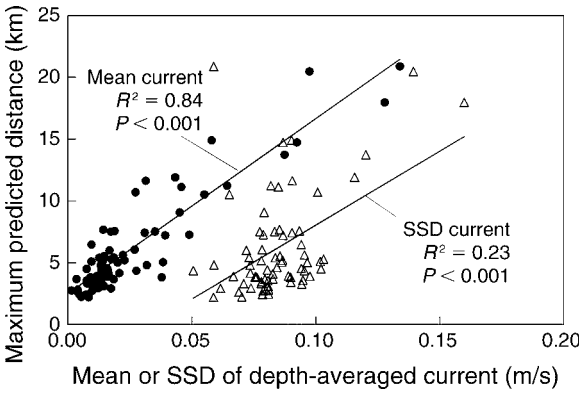

FIG. 10. Relationship between the maximum predicted dispersal distance during a deployment and two simple hydrodynamic indices. The solid circles indicate the pattern for the mean depth-averaged total current, and the open triangles indicate the pattern for the sum of the standard deviations (SSD) of the east–west and north–south depth-averaged currents.

DISCUSSION

Causes and consequences of noisy short-distance settlement

The observation that short-distance dispersal distributions exhibit appreciable spikiness and high levels of deployment-by-deployment variability (Figs. 3 and 4) suggests that these traits are intrinsic to processes involving fluid mixing. This is indeed likely the case. As Garrett (1983) has shown mathematically, when suspended material (like a patch of spores) is first released into a parcel of water, turbulence initially "stirs" the patch, stretching and smearing it, but not effectively "mixing" it to a smoothly varying concentration field. It is not until later that turbulence is able to mix suspended material into a less-discontinuous distribution. Horizontal transport by orbital wave motions further increases the complexity of this process. It is therefore to be expected that settlement near a source plant will produce a noisy distribution as spore-containing fluid filaments stochastically contact the seafloor.

Such issues of settlement variability have implications for understanding the sporadic appearance of individuals or small clumps of *Macrocystis* at large distances outside regions characterized by more uniform recruitment. Although dispersal distributions may become smoother the longer turbulence mixes spores (and thus the farther spores transit from their origin), some patchiness will persist into the tails of a distribution. This feature means that even at large distances where average spore densities consistently fall below the threshold for fertilization, there will still be occasions when local spore densities exceed the critical level. These less-common episodes of denser settlement complement those arising from long-distance dispersal associated with detached adult sporophytes that release spores as they drift with currents (Dayton et al. 1984, Macaya et al. 2005).

Scales of transport and distribution shape

The shapes of short-distance dispersal distributions also serve to emphasize the relevance of the spatial configuration of kelp beds, especially the relative dimensions of plant spacing vs. bed length or width. The predicted modal dispersal distance for spores released from a solitary plant is of order 1 m (Fig. 5a). Because this distance is much shorter than the typical length of a kelp forest (typically 100s of meters), summation of dispersal kernels from multiple plants causes high within-forest settlement (Fig. 6b). This effect likely exacerbates the strong density dependence that characterizes kelp demographics (Reed 1990, Reed et al. 1991), and that structures many kelp communities (Schiel and Choat 1980, Dayton et al. 1984, Reed and Foster 1984).

Other features of distribution shape may be exhibited to a greater or lesser extent under different circumstances, with situation-specific consequences. In terrestrial systems, single-plant sources produce dispersal kernels that peak a small distance from the origin. In contrast, terrestrial kernels from area sources yield dispersal curves with central broad peaks (Greene and Johnson 1996, Nathan et al. 2001). In our present study, the tendency for wave motions to obscure the central dip in the solitary kelp-plant distribution (Fig. 5a) suggests that solitary sources in marine systems may operate more similarly to area sources than might otherwise have been expected. This point holds additional weight given the pervasiveness of waves in coastal habitats. On the other hand, distinctions between point and area sources may continue to apply in locations where wave

TABLE 1. Maximum-likelihood parameter fits to the phenomenological representations of distance distributions predicted for an isolated source subjected to measured flow conditions.

Distribution or deployment	Parameters		
	a	*b*	*c*
Fits to distribution associated with all deployments lumped together			
2Dt	0.036	1.16	n.d.
Lognormal	2.22	95.5	n.d.
Lognormal–Gaussian	2.03	27.8	1060
Combined lognormal–Gaussian fits to individual deployments of Fig. 12a			
SKP 19	1.81	25.2	1940
SKP 32	1.72	18.9	1100
SKP 37	1.78	27.6	1430
KB 4	1.72	29.3	870
KB 10	1.72	21.3	720
KB 12	1.73	14.4	572
KB 15	1.84	25.1	2450

Note: Flow conditions correspond to those measured for deployments during the solitary kelp-plant experiment (SKP) and/or kelp-bed experiment (KB); n.d. = no data are possible.

effects are minor and currents are fast (e.g., in interior waterways like those of Puget Sound in the state of Washington, USA; Eckman et al. 2003). Differences in the shapes of dispersal distributions could then impact the accuracy of model projections of settlement, for example in the context of estimating probabilities of self-fertilization around sparsely arrayed individuals.

A phenomenological form for short- and long-distance dispersal

Fig. 11a demonstrates that traditional phenomenological expressions cannot adequately represent spore dispersal in *Macrocystis* across the entire range of distances for all hydrodynamic scenarios. This observation may relate to the fact that turbulence and wave-driven processes are more important in local spore transport, while currents dominate dispersal to greater distances. Such partitioning of flow effects is paralleled by the tendency for short- and long-distance regions of the predicted distributions to be best represented by lognormal and Gaussian forms, respectively (Fig. 11). This point suggests that an alternative, composite expression may be worth considering, with

$$p(r) = \frac{1}{2a\sqrt{2\pi}r}\exp\left[-\frac{(\ln r - \ln b)^2}{2a^2}\right] + \frac{1}{c\sqrt{2\pi}}\exp\left(-\frac{r^2}{2c^2}\right) \quad (11)$$

where a, b, and c are fitted parameters. Eq. 11 represents the sum of a lognormal and a normal probability density function, each scaled to ensure that their sum integrates to 1.

Compared to standard 2Dt or lognormal distributions, the average lognormal-Gaussian expression tracks the band of predicted distributions far better (Fig. 11a). Moreover, if the parameter c in Eq. 11 is allowed to vary, even deployment-by-deployment distributions can be represented by the lognormal–Gaussian phenomenological form (Fig. 12a). This property is particularly appropriate because the parameter c is connected to the mean current velocity (Fig. 12b). Such a relationship reaffirms the dependence of long-distance dispersal on regional flow processes, and provides a means of parameterizing dispersal via an accessible oceanographic index.

Benchmark relationships revealed by the phenomenological distribution

The development of a phenomenological expression suitable for representing both short- and long-distance dispersal is a primary objective of this study. In this section, we demonstrate via three examples how the lognormal–Gaussian distribution informs issues in kelp ecology. Although our examinations are broad stroke in character and therefore not complete evaluations, they provide insights that are useful as points of departure for future work. We focus in particular on topics related to population dynamics and structure.

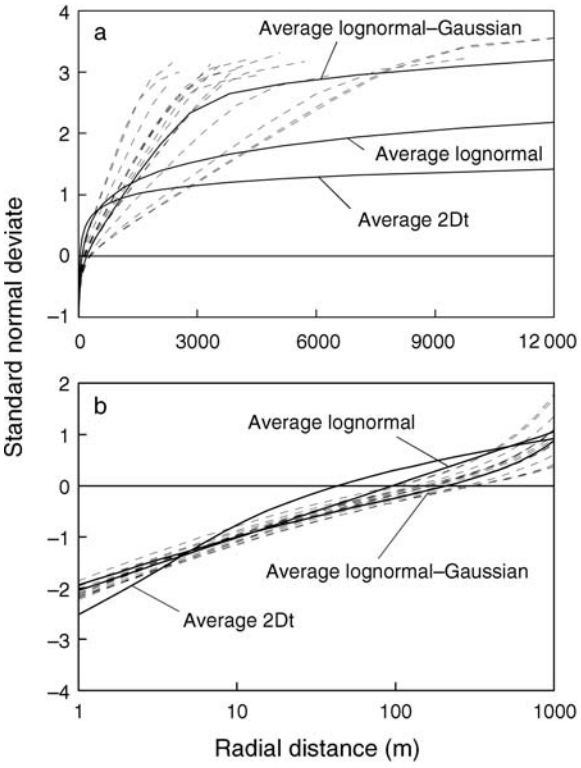

FIG. 11. Degree of fit of phenomenological dispersal curves to dispersal patterns predicted by the physically based model. Model results (dashed lines) were computed assuming single-plant sources exposed to flow conditions characterizing the solitary kelp-plant and kelp-bed deployments. Solid lines correspond to the average phenomenological curve fits to model results lumped across all deployments from both experiments. (a) Complete cumulative distributions spanning the entire range of dispersal, with the y-axis depicted on a probability (Z value) scale and the x-axis on a linear scale. Note that the tails of the distributions are nearly linear, which suggests a Gaussian character. (b) Cumulative probability distributions spanning only the short-distance portion of the distributions, with the y-axis depicted on a probability (Z value) scale and the x-axis on a logarithmic scale. Note that the short-distance region is nearly linear when plotted in this manner, which suggests a lognormal character.

Rates of spore release.—A first step in linking fluid flow to population-level analyses is assessing the rate of input of new propagules, which in kelps is related to rates of spore release. Although rough estimates of such rates have been available for some time (e.g., Anderson and North 1967; see also Graham 2002, 2003), there has been little ability to bound these estimates, particularly under field conditions. Here we compare measured spore densities on microscope slides from the solitary kelp-plant array to predicted probabilities acquired by integrating (over the area of each slide at each slide location) the two-dimensional probability density function that results from dividing the average lognormal–Gaussian expression by $2\pi r$ (Nathan and Muller-Landau 2000). The ratio of measured density to predicted probability at each location yields an estimate

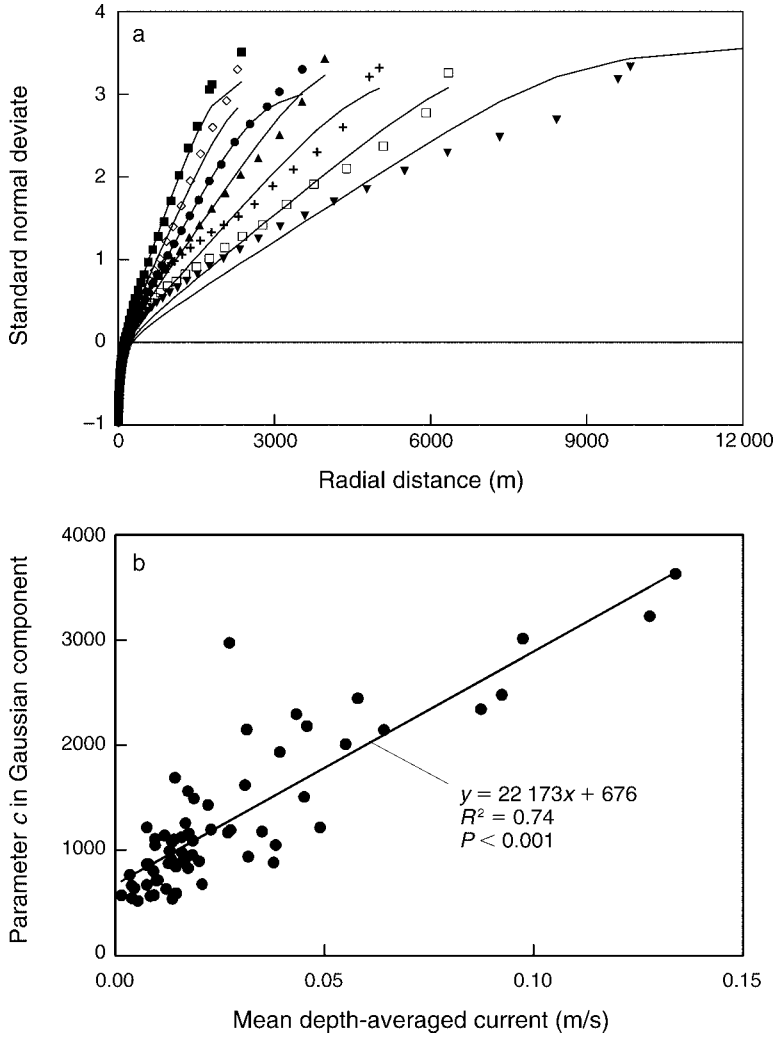

FIG. 12. Curve fits of the combined lognormal–Gaussian distribution to the model-predicted results. (a) Demonstration that the phenomenological distribution provides a reasonable match in both short- and long-distance regions. Different symbols indicate predictions from different deployments, as noted in Table 1. Only a subset of the distributions are graphed to maintain clarity. (b) Relationship of parameter c in the lognormal–Gaussian distribution to the mean depth-averaged total current speed.

of the number of female spores released by the source plant during an experimental deployment (recall that male spores were not counted in the microscope analyses). The linear trend in Fig. 13 indicates that such estimates are consistent across sampling distances, allowing the slope of the regression to operate as a robust average measure of release rate. This approach suggests that 10^8 female spores were released per individual over a two-day interval, or assuming an unbiased sex ratio, 10^8 total spores per individual per day. Although this simple calculation ignores important factors such as spore and gametophyte mortality and variation in fecundity among individuals (Reed et al. 1994, 1997), it provides a first-order estimate suitable for guiding other studies.

Long-distance dispersal and population connectivity.— The above rate of spore release also enables estimation of the maximal distance from a source at which spore densities sufficient to allow routine fertilization (and thereby routine recruitment) might be expected. Such distances are difficult to determine using traditional field methods that monitor the appearance of new individuals due to the challenge of ascertaining the sources of spores for specific recruits. Such issues are further complicated by uncertainties regarding the durations over which gamete-producing gametophyte stages that develop from spores remain fertile. Field experiments indicate that gametophytes often survive only a few days (Reed et al. 1988, 1994), while laboratory studies suggest that gametophytes can be viable for weeks or more (Deysher and Dean 1984). If extended gametophyte viability occurs in some habitats (e.g., Ladah et al. 1999), aggregate levels of spores accumulating over multiple days may be what determine whether threshold densities

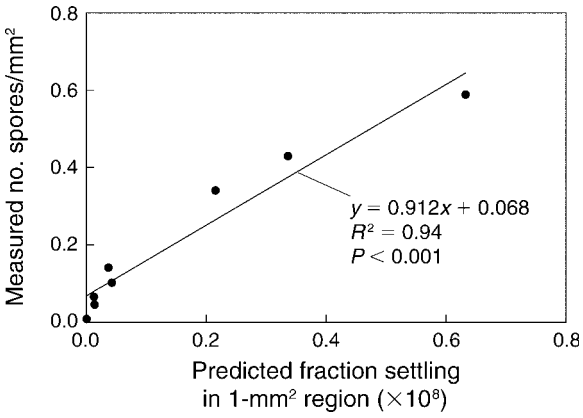

FIG. 13. Relationship between the fraction of spores released from a solitary plant that would be predicted to settle in a 1-mm^2 region at the location of a particular slide collector in the field, and the measured number of spores per square millimeter settling on that slide. Each point corresponds to data from a single slide position during the solitary kelp-plant experiment. (Values on the *x*-axis have been multiplied by 10^8; i.e., 0.8 on the scale is actually 0.000000008.) The linear trend among data points indicates that calculated rates of spore release are consistent among slide positions and can be estimated by the slope of the line.

for fertilization are reached, and thus whether recruitment can occur. Clearly, the size of the adult population contributing to spore accumulation will also play a role.

To account for both the number of plants and any accumulation of spores and gametophytes, we define the magnitude of a spore source as the product of plant number and accumulation time. This representation does not address processes promoting synchronous spore release (Reed et al. 1997) or any effect that position in a forest might have. Such issues are complex and are therefore neglected here in order to isolate core relationships. Given these simplifications and the assumption of a release rate of 10^8 spores per individual per day, the integral of the two-dimensional form of the average lognormal–Gaussian expression predicts densities of spore settlement across distance. Applying the additional criterion of a minimum density for fertilization of 1 spore/mm^2, predictions of maximal recruitment distance ensue. These distances vary as a function of source magnitude and current speed (Fig. 14). Of particular note is a region of transition apparent at 1500–2000 m, beyond which substantially greater source magnitudes are required to extend maximal recruitment distances, especially when currents are slow.

Values on the *x*-axis of Fig. 14 can be interpreted by considering typical dimensions and plant densities in kelp forests. Kelp beds commonly span 500 m alongshore and 300 m cross-shore, and although plant densities are highly variable, values of order 0.1 individuals/m^2 of seafloor are not unusual (B. Gaylord, J. H. Rosman, D. C. Reed, J. R. Koseff, J. Fram, S. MacIntyre, K. Arkema, C. McDonald, J. L. Largier, M. A. Brzezinski, P. T. Raimondi, S. G. Monismith, and B. Mardian, *unpublished manuscript*). A kelp bed with these characteristics would contain 15 000 plants. If spores and gametophytes from these plants accumulated for one week before becoming infertile, this forest would have a source magnitude of 1×10^5. The massive Point Loma bed in San Diego, California, USA (10 km long $\times$ 1 km wide; Dayton et al. 1984) would, by comparison, have a source magnitude approaching 10^7, assuming the same plant density. Given that most kelp forests fall on the smaller end of the spectrum, scales of connectivity of

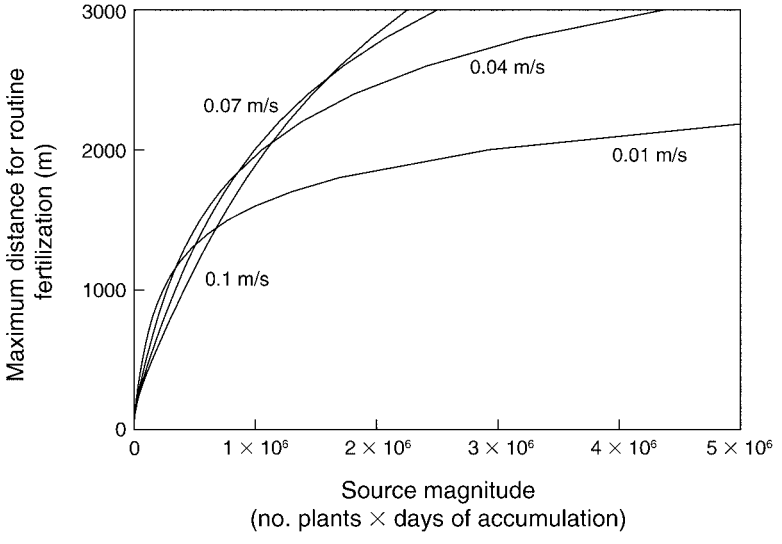

FIG. 14. Predicted maximal distances from a source at which spores can be expected to settle at sufficient densities to enable fertilization and therefore recruitment, as a function of the magnitude of the spore source and the average current speed. The source magnitude is calculated as the product of the number of kelp individuals that contribute spores at a rate of 10^8 spores/d and the number of days over which fertile gametophytes arising from spores accumulate.

order 1 km may be fairly representative (Fig. 14). We emphasize, however, that although such scales can be useful for conceptualizing spatial relationships among kelp patches, the point-source approximation underlying the lognormal–Gaussian expression becomes increasingly violated as recruitment distances get smaller relative to dimensions of the forest. The curves of Fig. 14 should therefore be viewed as trendlines rather than precise descriptors.

Rates of self-fertilization.—Raimondi et al. (2004) demonstrated that inbreeding in *Macrocystis* can have substantial impacts on lifetime fitness. Given that the modal dispersal distance in *Macrocystis* is predicted to be of order 1 m (Fig. 5a), which is similar to the spacing between individuals within a forest (often 1–10 m), a sizeable fraction of propagules settling near an adult are likely to be its own spores. In this context, the lognormal–Gaussian expression is useful for estimating rates of self-fertilization.

A first examination of selfing in kelp forests proceeds as follows. We assume that gametes only interact (and thus fertilize) if they derive from spores landing within the same 1-mm^2 region, consistent with the known density threshold. We also assume that all adults release spores at the same rate. Although this simplification is often violated in nature, it represents the default case. The two-dimensional form of the phenomenological dispersal expression can then be integrated, this time over many 1-mm^2 regions across a grid surrounding several model adults. Within each 1-mm^2 region, the fraction of spores derived from a specific plant is given by the probability that a spore from that plant lands in the region, divided by the sum of the probabilities from it and any other adults that contribute spores. The probability of self-fertilization is computed from these fractions as

$$P_{\text{selfing}} = \sum_{i=1}^{n} (f_i)^2 \qquad (12)$$

where f_i is the fraction of spores produced by adult i, and spores are contributed by n adults (Raimondi et al. 2004).

Spatial patterns of self-fertilization can be examined for an idealized distribution of plants by imagining a square sector of seafloor extracted from the center of a kelp forest. This sector has an adult plant located at each of its corners and another at its center. Each of these plants releases spores from sporophylls that sweep about in flow, a process mimicked using point-source releases from 50 randomly distributed locations within a 1-m-wide annulus surrounding each adult. The mean dispersal distributions from these 50 releases are then computed and probabilities of selfing within the idealized kelp sector are calculated using Eq. 12. Depending on the spacing between individuals, predicted selfing probabilities range from ~20% to >40% (Fig. 15), with peak values increasing as the distance between individuals rises. These patterns vary only imperceptibly with hydrodynamic conditions because, for closely settling spores, the smearing effects of many (instantaneously large) bidirectional currents and waves overwhelm the effects of a (small residual) mean flow that operates on each spore only briefly. This finding does not mean that observed reductions of flow within kelp forests are irrelevant for affecting rates of self-fertilization. Both mean currents and standard deviations of currents are altered within kelp beds (e.g., Jackson and Winant 1983, Jackson 1998; B. Gaylord, J. H. Rosman, D. C. Reed, J. R. Koseff, J. Fram, S. MacIntyre, K. Arkema, C. McDonald, J. L. Largier, M. A. Brzezinski, P. T. Raimondi, S. G. Monismith, and B. Mardian, *unpublished manuscript*), and parameters a and b in the lognormal-Gaussian distribution are weak functions of the sum of the standard deviations of depth-averaged east–west and north–south currents ($P < 0.005$ for both regressions). Given complexities such as these, values in Fig. 15 are probably best interpreted as support for order 10% (as opposed to 1% or 0.1%) rates of self-fertilization in kelp forests. Such rough estimates may provide a baseline for more detailed demographic studies or genetic evaluations of algal population structure.

Caveats and conclusions

The above results provide insight into *Macrocystis* spore dispersal and nearshore propagule transport more generally. Several potential limitations, however, must be kept in mind. In particular, model predictions through long-distance regions cannot yet be tested due to an absence of empirical data. This point bears on the most serious simplification of the model, which is an assumption of "slab-type" fluid motion. Flow conditions measured at the field site are applied as if they hold regionally, which ignores spatial variability in oceanographic conditions. As a consequence, although predictions regarding the tails of the distributions provide as good an estimate as is possible using presently available methods, they must be viewed as tentative. A second neglected factor is water stratification. Although freshwater input into surrounding areas is typically low except during isolated rain events in southern California, thermal stratification is often present during the summer and fall and can alter profiles of vertical mixing. However, there is no indication that model predictions were worse during summer as compared to winter and spring when stratification was weak or absent. Third, as alluded to in the preceding section, we have ignored any effects that kelps themselves might have on flow (Jackson and Winant 1983, Koehl 1986, Eckman et al. 1989, Jackson 1998, Stevens et al. 2001, Gaylord et al. 2003, 2004; B. Gaylord, J. H. Rosman, D. C. Reed, J. R. Koseff, J. Fram, S. MacIntyre, K. Arkema, C. McDonald, J. L. Largier, M. A. Brzezinski, P. T. Raimondi, S. G. Monismith, and B. Mardian, *unpublished manuscript*).

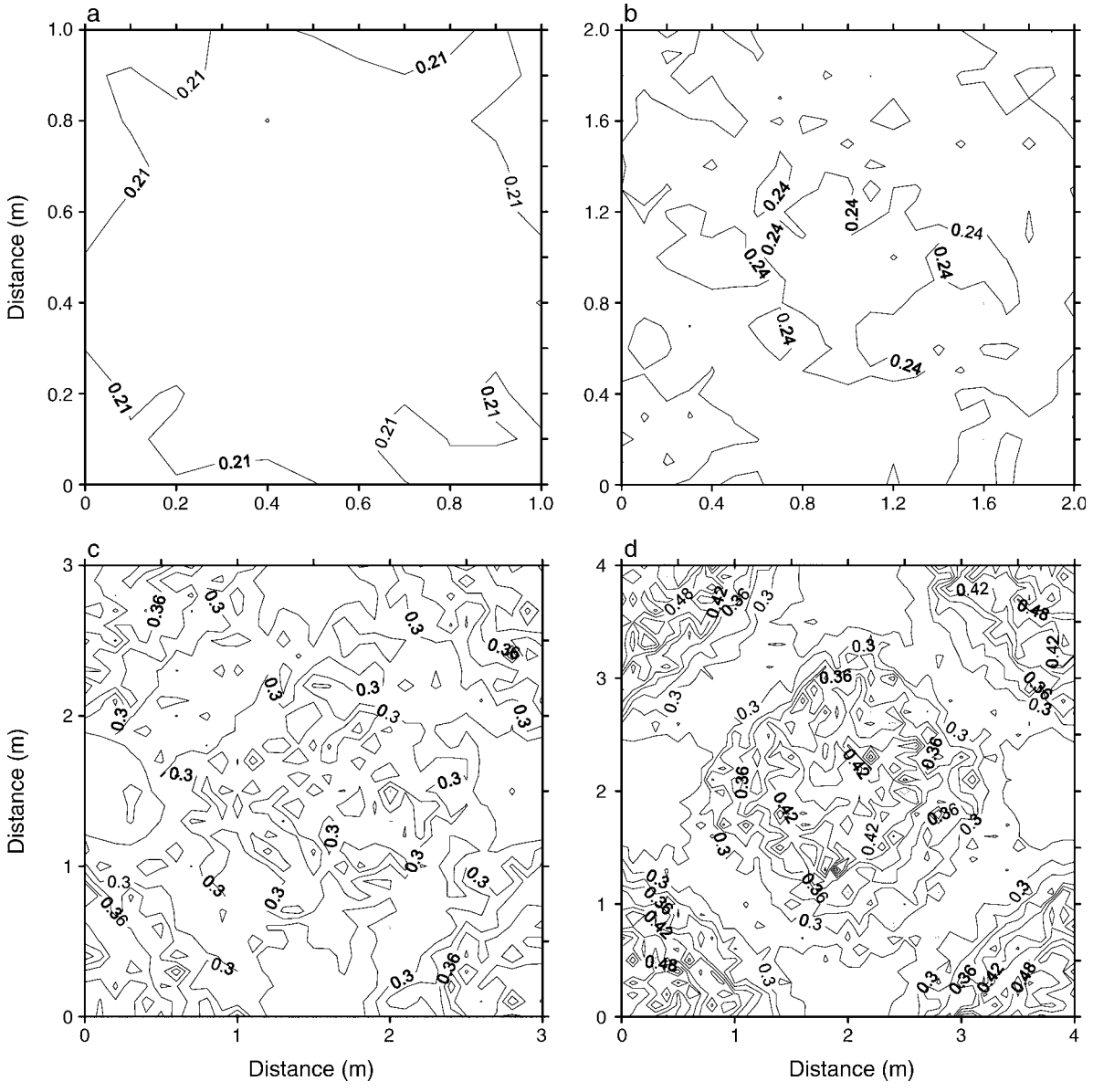

FIG. 15. Predicted probabilities of self-fertilization, depicted as proportions of 1.0, in an idealized kelp-forest sub-unit. Kelp individuals are assumed to be located at each corner of the square regions shown, and in the center of the squares. The distance between plants varies across the four panels, yielding nearest-neighbor distances of (a) 0.7 m, (b) 1.4 m, (c) 2.1 m, and (d) 2.8 m. Probability contours are calculated assuming a current speed of 0.05 m/s, although results are not sensitive to this parameter. Note that in panel (a) the selfing rate in the center of the sector is slightly lower (0.20) than the rate of 0.21 predicted for corner regions. This minor artifact is also apparent in the other panels and arises because corner regions receive spores from only one adjacent quadrant, rather than from all directions in the idealized sectors.

Although temporally averaged dispersal patterns in short-distance (and thus within-forest) regions appear moderately insensitive to mean hydrodynamic conditions, future work will need to address plant–flow interactions in order for a complete understanding of dispersal in this system to be achieved.

Despite such simplifications, the core findings of the study are likely to remain robust. Dispersal is indeed a variable process controlled by interactions of turbulent mixing with currents and waves (and in species that swim faster than algal spores, behavior). Even in the face of complex hydrodynamic processes, phenomenological representations of nearshore dispersal can be formulated. It appears possible to explicitly connect such representations back to basic physical factors that broadly influence ecological pattern in marine communities. In the case of giant kelp, this approach appears valuable for examining a number of fundamental processes, including rates of spore release, population connectivity, and levels of inbreeding.

Acknowledgments

We thank two anonymous reviewers for helpful comments, M. Anghera for field work, C. Gotshalk for analytical support, and S. McLean for technical advice. This research was funded by NSF grants OCE96-33329, OCE99-82105, and OCE02-41447, and is contribution number 214 of the Partnership for Interdisciplinary Studies of Coastal Oceans (PISCO): a long-term ecological consortium funded by the David and Lucille Packard Foundation. This work is also contribution number 2348 from the Bodega Marine Laboratory, University of California–Davis.

Literature Cited

Anderson, E. K., and W. J. North. 1966. *In situ* studies of spore production and dispersal in the giant kelp, *Macrocystis*. Pages 73–86 *in* E. G. Young and J. L. McLachlan, editors. Proceedings of the Fifth International Seaweed Symposium, 25–28 August 1965 (Halifax, Nova Scotia). Pergamon Press, New York New York, USA.

Anderson, E. K., and W. J. North. 1967. Zoospore release rates in the giant kelp *Macrocystis*. Bulletin of the Southern California Academy of Sciences **66**:223–232.

Anderson, M. 1991. Mechanistic models for the seed shadows of wind-dispersed plants. American Naturalist **137**:476–497.

Clark, J. S., M. Lewis, and L. Horvath. 2001. Invasion by extremes: population spread with variation in dispersal and reproduction. American Naturalist **157**:537–554.

Clark, J. S., M. Silman, R. Kern, E. Macklin, and J. HillerRisLambers. 1999. Seed dispersal near and far: patterns across temperate and tropical forests. Ecology **80**:1475–1494.

Clauser, F. H. 1956. The turbulent boundary layer. Advances in Applied Mechanics **4**:1–51.

Cowen, R. K., K. M. M. Lwiza, S. Sponaugle, C. B. Paris, and D. B. Olson. 2000. Connectivity of marine populations: open or closed? Science **287**:857–859.

Dayton, P. K., V. Currie, T. Gerrodette, B. D. Keller, R. Rosenthal, and D. Ven Tresca. 1984. Patch dynamics and stability of some California kelp communities. Ecological Monographs **54**:253–289.

Dayton, P. K., and M. J. Tegner. 1984. Catastrophic storms, El Niño, and patch stability in a southern California kelp community. Science **224**:283–285.

Dayton, P. K., M. J. Tegner, P. E. Parnell, and P. B. Edwards. 1992. Temporal and spatial patterns of disturbance and recovery in a kelp forest community. Ecological Monographs **62**:421–445.

Denny, M. W. 1988. Biology and the mechanics of the wave-swept environment. Princeton University Press, Princeton, New Jersey, USA.

Deysher, L. E., and T. A. Dean. 1984. Critical irradiance levels and the interactive effects of quantum irradiance and dose on gameogenesis in the giant kelp, *Macrocystis pyrifera*. Journal of Phycology **20**:520–524.

DiBacco, C., and L. A. Levin. 2000. Development and application of elemental fingerprinting to track the dispersal of marine invertebrate larvae. Limnology and Oceanography **45**:871–880.

Duggins, D. O., C. A. Simenstad, and J. A. Estes. 1989. Magnification of secondary production by kelp detritus in coastal marine ecosystems. Science **245**:170–173.

Ebeling, A. W., D. R. Laur, and R. J. Rowley. 1985. Severe storm disturbances and reversal of community structure in a southern California kelp forest. Marine Biology **84**:287–294.

Eckman, J. E. 1990. A model of passive settlement by planktonic larvae onto bottoms of different roughness. Limnology and Oceanography **35**:887–901.

Eckman, J. E., D. O. Duggins, and A. T. Sewell. 1989. Ecology of understory kelp environments. I. Effects of kelps on flow and particle transport near the bottom. Journal of Experimental Marine Biology and Ecology **129**:173–187.

Eckman, J. E., D. O. Duggins, and C. E. Siddon. 2003. Current and wave dynamics in the shallow subtidal: implications to the ecology of understory and surface-canopy kelps. Marine Ecology Progress Series **264**:45–56.

Edwards, M. S. 2004. Estimating scale-dependency in disturbance impacts: El Niños and giant kelp forests in the northeast Pacific. Oecologia **138**:436–447.

Emery, W. J., and R. E. Thomson. 2001. Data analysis methods in physical oceanography. Second edition. Elsevier Science, New York, New York, USA.

Garland, E. D., C. A. Zimmer, and S. J. Lentz. 2002. Larval distributions in inner-shelf waters: the roles of wind-driven cross-shelf currents and diel vertical migrations. Limnology and Oceanography **47**:803–817.

Garrett, C. 1983. On the initial streakiness of a dispersing tracer in two- and three-dimensional turbulence. Dynamics of Atmospheres and Oceans **7**:265–277.

Gaylord, B. 1999. Detailing agents of physical disturbance: wave-induced velocities and accelerations on a rocky shore. Journal of Experimental Marine Biology and Ecology **239**:85–124.

Gaylord, B., C. A. Blanchette, and M. W. Denny. 1994. Mechanical consequences of size in wave-swept algae. Ecological Monographs **64**:287–313.

Gaylord, B., M. W. Denny, and M. A. R. Koehl. 2003. Modulation of wave forces on kelp canopies by alongshore currents. Limnology and Oceanography **48**:860–871.

Gaylord, B., and S. D. Gaines. 2000. Temperature or transport? Range limits in marine species mediated solely by flow. American Naturalist **155**:769–789.

Gaylord, B., D. C. Reed, P. T. Raimondi, L. Washburn, and S. R. McLean. 2002. A physically based model of macroalgal spore dispersal in the wave and current-dominated nearshore. Ecology **83**:1239–1250.

Gaylord, B., D. C. Reed, L. Washburn, and P. T. Raimondi. 2004. Physical–biological coupling in spore dispersal of kelp forest macroalgae. Journal of Marine Systems **49**:19–39.

Graham, M. H. 2002. Prolonged reproductive consequences of short-term biomass loss in seaweeds. Marine Biology **140**: 901–911.

Graham, M. H. 2003. Coupling propagule output to supply at the edge and interior of a giant kelp forest. Ecology **84**:1250–1264.

Grant, W. D., and O. S. Madsen. 1986. The continental-shelf bottom boundary layer. Annual Review of Fluid Mechanics **18**:265–305.

Greene, D. F., C. D. Canham, K. D. Coates, and P. T. Lepage. 2004. An evaluation of alternative dispersal functions for trees. Journal of Ecology **92**:758–766.

Greene, D. F., and E. A. Johnson. 1989. A model of wind dispersal of winged or plumed seeds. Ecology **70**:339–347.

Greene, D. F., and E. A. Johnson. 1996. Wind dispersal of seeds from a forest into a clearing. Ecology **77**:595–609.

Grosberg, R. K., and C. W. Cunningham. 2001. Genetic structure in the sea: from populations to communities. Pages 60–84 *in* M. D. Bertness, S. D. Gaines, and M. E. Hay, editors. Marine community ecology. Sinauer Associates, Sunderland, Massachusetts, USA.

Harms, S., and C. D. Winant. 1998. Characteristic patterns of the circulation in the Santa Barbara Channel. Journal of Geophysical Research **103**:3041–3065.

Harrold, C., and D. C. Reed. 1985. Food availability, sea urchin grazing, and kelp forest community structure. Ecology **66**:1160–1169.

Jackson, G. A. 1998. Currents in the high drag environment of a coastal kelp stand off California. Continental Shelf Research **17**:1913–1928.

Jackson, G. A., and C. D. Winant. 1983. Effect of a kelp forest on coastal currents. Continental Shelf Research **2**:75–80.

Kinlan, B. P., and S. D. Gaines. 2003. Propagule dispersal in marine and terrestrial environments: a community perspective. Ecology **84**:2007–2020.

Koehl, M. A. R. 1986. Seaweeds in moving water: form and mechanical function. Pages 603–634 *in* T. J. Givnish, editor. On the economy of plant form and function. Cambridge University Press, Cambridge, UK.

Ladah, L. B., J. A. Zertuche-Gonzalez, and G. Hernandez-Carmona. 1999. Giant kelp (*Macrocystis pyrifera*, Phaeophyceae) recruitment near its southern limit in Baja California after mass disappearance during ENSO 1997–1998. Journal of Phycology **35**:1106–1112.

Leichter, J. J., S. R. Wing, S. L. Miller, and M. W. Denny. 1996. Pulsed delivery of subthermocline water to Conch Reef (Florida Keys) by internal tidal bores. Limnology and Oceanography **41**:1490–1501.

Levin, S. A., H. C. Muller-Landau, R. Nathan, and J. Chave. 2003. The ecology and evolution of seed dispersal: a theoretical perspective. Annual Review of Ecology and Systematics **34**:575–604.

Lockwood, D. R., A. Hastings, and L. W. Botsford. 2002. The effects of dispersal patterns on marine reserves: Does the tail wag the dog? Theoretical Population Biology **61**:297–309.

Macaya, E. C., S. Boltana, I. A. Hinojosa, J. E. Macchiavello, N. A. Valdivia, N. R. Vasquez, A. H. Buschmann, J. A. Vasquez, J. M. Alonso Vega, and M. Thiel. 2005. Presence of sporophylls in floating kelp rafts of *Macrocystis* spp. (Phaeophyceae) along the Chilean Pacific coast. Journal of Phycology **41**:913–922.

McNair, J. N., J. D. Newbold, and D. D. Hart. 1997. Turbulent transport of suspended particles and dispersing benthic organisms: How long to hit bottom? Journal of Theoretical Biology **188**:29–52.

Monismith, S., and D. Fong. 2004. A note on the potential transport of scalars and organisms by surface waves. Limnology and Oceanography **29**:1214–1217.

Nathan, R., G. G. Katul, H. S. Horn, S. M. Thomas, R. Oren, R. Avissar, S. W. Pacala, and S. A. Levin. 2002. Mechanisms of long-distance dispersal of seeds by wind. Nature **418**:409–413.

Nathan, R., and H. C. Muller-Landau. 2000. Spatial patterns of seed dispersal, their determinants and consequences for recruitment. Trends in Ecology and Evolution **15**:278–285.

Nathan, R., U. N. Safriel, and I. Noy-Meir. 2001. Field validation and sensitivity analysis of a mechanistic model for tree seed dispersal by wind. Ecology **82**:374–388.

Neushul, M. 1963. Studies on the giant kelp, *Macrocystis*. II. Reproduction. American Journal of Botany **50**:354–359.

North, W. J. 1971. The biology of giant kelp beds (*Macrocystis*) in California. Verlag Von J. Cramer, Lehre, Germany.

Okubo, A., and S. A. Levin. 1989. A theoretical framework for data analysis of wind dispersal of seeds and pollen. Ecology **70**:329–338.

Palumbi, S. R. 1995. Using genetics as an indirect estimator of larval dispersal. Pages 369–387 *in* L. McEdward, editor. Ecology of marine invertebrate larvae. CRC Press, Gainesville, Florida, USA.

Pineda, J. 1991. Predictable upwelling and the shoreward transport of planktonic larvae by internal tidal bores. Science **253**:548–551.

Possingham, H. P., and J. Roughgarden. 1990. Spatial population dynamics of a marine organism with a complex life cycle. Ecology **71**:973–985.

Raimondi, P. T., D. C. Reed, B. Gaylord, and L. Washburn. 2004. Effects of self-fertilization in the giant kelp, *Macrocystis pyrifera*. Ecology **85**:3267–3276.

Reed, D. C. 1990. The effects of variable settlement and early competition on patterns of kelp recruitment. Ecology **71**:776–787.

Reed, D. C., T. W. Anderson, A. W. Ebeling, and M. Anghera. 1997. The role of reproductive synchrony in the colonization potential of kelp. Ecology **77**:300–316.

Reed, D. C., A. W. Ebeling, T. W. Anderson, and M. Anghera. 1996. Differential reproductive responses to fluctuating resources in two seaweeds with different reproductive strategies. Ecology **77**:300–316.

Reed, D. C., and M. S. Foster. 1984. The effects of canopy shading on algal recruitment and growth in a giant kelp forest. Ecology **65**:937–948.

Reed, D. C., B. P. Kinlan, P. T. Raimondi, L. Washburn, B. Gaylord, and P. T. Drake. 2006. A metapopulation perspective on patch dynamics and connectivity of giant kelp. Pages 353–381 *in* J. P. Kritzer and P. F. Sale, editors. Marine metapopulations. Academic Press, San Diego, California, USA.

Reed, D. C., D. R. Laur, and A. W. Ebeling. 1988. Variation in algal dispersal and recruitment: the importance of episodic events. Ecological Monographs **58**:321–335.

Reed, D. C., R. J. Lewis, and M. Anghera. 1994. Effects of an open-coast oil-production outfall on patterns of giant kelp (*Macrocystis pyrifera*) recruitment. Marine Biology **120**:25–31.

Reed, D. C., M. Neushul, and A. W. Ebeling. 1991. Role of settlement density on gametophyte growth and reproduction in the kelps *Pterygophora californica* and *Macrocystis pyrifera* (Phaeophyceae). Journal of Phycology **27**:361–366.

Reed, D. C., S. C. Schroeter, and P. T. Raimondi. 2004. Spore supply and habitat availability as sources of recruitment limitation in the giant kelp *Macrocystis pyrifera* (Phaeophyceae). Journal of Phycology **40**:275–284.

Richards, S. A., H. P. Possingham, and B. J. Noye. 1995. Larval dispersion along a straight coast with tidal currents: complex distribution patterns from a simple model. Marine Ecology Progress Series **122**:59–71.

Roughgarden, J., S. Gaines, and H. Possingham. 1988. Recruitment dynamics in complex life cycles. Science **241**:1460–1466.

Schiel, D. R., and J. H. Choat. 1980. Effects of density on monospecific stands of marine algae. Nature **285**:324–326.

Seymour, R. J., M. J. Tegner, P. K. Dayton, and P. E. Parnell. 1989. Storm wave induced mortality of giant kelp, *Macrocystis pyrifera*, in Southern California. Estuarine Coastal and Shelf Science **28**:277–292.

Shanks, A. L. 1995. Mechanisms of cross-shelf dispersal of larval invertebrates and fish. Pages 323–367 *in* L. R. McEdward, editor. Ecology of marine invertebrates. CRC Press, Boca Raton, Florida, USA.

Siegel, D. A., B. P. Kinlan, B. Gaylord, and S. D. Gaines. 2003. Lagrangian descriptions of marine larval dispersion. Marine Ecology Progress Series **260**:83–96.

Sokal, R. R., and F. J. Rohlf. 1995. Biometry. Third edition. W. H. Freeman and Company, New York, New York, USA.

Soons, M. B., G. W. Heil, R. Nathan, and G. G. Katul. 2004. Determinants of long-distance seed dispersal by wind in grasslands. Ecology **85**:3056–3068.

Sotka, E. E., J. P. Wares, J. A. Barth, R. K. Grosberg, and S. R. Palumbi. 2004. Strong genetic clines and geographical variation in gene flow in the rocky intertidal barnacle *Balanus glandula*. Molecular Ecology **13**:2143–2156.

Stevens, C. L., C. L. Hurd, and M. J. Smith. 2001. Water motion relative to subtidal kelp fronds. Limnology and Oceanography **46**:668–678.

Stoyan, D., and S. Wagner. 2001. Estimating the fruit dispersion of anemochorous forest trees. Ecological Modelling **145**:35–47.

Swearer, S. E., J. E Caselle, D. W. Lea, and R. R. Warner. 1999. Larval retention and recruitment in an island population of a coral-reef fish. Nature **402**:799–802.

Tackenberg, O. 2003. Modeling long-distance dispersal of plant diaspores by wind. Ecological Monographs **73**:173–189.

Wares, J. P., S. D. Gaines, and C. W. Cunningham. 2001. A comparative study of asymmetric migration events across a marine biogeographic boundary. Evolution **55**:295–306.

Washburn, L., S. Stone, and S. MacIntyre. 1999. Dispersion of produced water in a coastal environment and its biological implications. Continental Shelf Research **19**:57–78.

Wiberg, P., and J. D. Smith. 1983. A comparison of field data and theoretical models for wave–current interactions at the bed on the continental shelf. Continental Shelf Research **2**: 147–162.

Wing, S. R., L. W. Botsford, S. V. Ralston, and J. L. Largier. 1998. Meroplankton distribution and circulation in a coastal retention zone of the northern California upwelling system. Limnology and Oceanography **43**:1710–1721.

Wing, S. R., J. L. Largier, L. W. Botsford, and J. F. Quinn. 1995. Settlement and transport of benthic invertebrates in an intermittent upwelling region. Limnology and Oceanography **40**:316–329.

Wormersley, H. B. S. 1954. The species of *Macrocystis* with special reference to those on southern Australian coasts. University of California Publications in Botany **27**:109–132.

Zacherl, D. C., P. H. Manriquez, G. Paradis, R. W. Day, J. C. Castilla, R. R. Warner, D. W. Lea, and S. D. Gaines. 2003. Trace elemental fingerprinting of gastropod statoliths to study larval dispersal trajectories. Marine Ecology Progress Series **248**:297–303.

APPENDIX A

A sketch of model components related to boundary-layer hydrodynamics (*Ecological Archives* M076-018-A1).

APPENDIX B

Field-measured spore data from the remaining solitary kelp-plant deployments not shown in Fig. 4a of the text (*Ecological Archives* M076-018-A2).

APPENDIX C

Field-measured spore data from the remaining kelp-bed deployments not shown in Fig. 4b of the text (*Ecological Archives* M076-018-A3).